



OmniVis
Business Plan

280 Utah Avenue, STE 200

South San Francisco, CA 94080

+1-415-938-4300

kclayton@omnivistech.com

<https://www.omnivistech.com>



Table of Contents

1. Executive Summary	3
2. Company Description	4
3. Market Analysis	5
4. Organization & Management	7
5. Products & Services	8
6. Marketing & Sales	10
7. Operations	12
8. Financials	13
A. Income Statement	14
B. Cash Flow Statement	15
C. Break-Even Analysis	16
D. Balance Sheet	17
9. Appendix	18



1. Executive Summary

Problem: Current infectious disease detection platforms are time intensive, costly, and imprecise, exacerbating widescale disease outbreaks worldwide. Cholera causes approximately 5M cases across the globe each year and wastes \$2 billion annually in treatments and lost productivity that could be avoidable through early detection.

Solution: OmniVis' hardware device and disposable test kit (razor/razor blade model) reduces the detection process from >24 hours down to 30 minutes, more accurately and affordably than other solutions. Additionally, OmniVis' data gathering & reporting tools provide insights over disease hotspots; enabling earlier warning before widescale outbreaks occur.

Market: For cholera, OmniVis will focus on selling to humanitarian aid organizations and water testing laboratories in emerging markets who are currently spending \$1.6B using sub-par test kits. We have 5 letters of intent from customers pending the confirmation of our technology. Our advantages are speed, portability, ease-of-use, and potential for expansion.

Competition: Current cholera competitors have significant failings: existing pathogen-culture methods require a 5-day processing time and cannot accurately detect low concentrations of the disease. All competitors require a clinical lab for testing, a significant obstacle in rural communities and emerging markets.

Business Model: OmniVis will leverage weaknesses in the existing testing market. Revenue streams include initial hardware investments (\$1000 per user) and recurring revenue of individual test kits (\$10 each). Due to the low initial costs (1/2 the start-up cost, 1/10th the cost per test), the expected volume of testing, the quality of our product and interdependence of hardware and testing kits, we expect a high level of volume and long-term customer loyalty.

Go-To-Market: We performed field tests in Bangladesh twice in 2019 for our cholera platform and are moving toward clinical trials for our COVID-19 test. We will start cholera sales in Q1 2022 and submit our solution for WHO pre-qualification. For growth, we will expand into blood-based clinical testing such as with HIV. As we prepare to enter the patient testing market, we will complete an FDA pre-submission.

Progress to Date: OmniVis was formed on October 2017 and transitioned to a C-Corp in June 2020. We have participated in two accelerator programs, been featured on news outlets like NPR, and TechCrunch and won a series of grants and awards. OmniVis has funded themselves through nondilutive grants and award money, raising \$3.16M.



2. Company Description

Mission Statement

OmniVis' mission is to create rapid detection technology that equips communities around the globe with the power and knowledge to protect their health.

Company History

OmniVis started in 2017 as a Purdue University spin-out in West Lafayette, IN. Our founders come from the School of Mechanical Engineering and Weldon School of Biomedical Engineering.

Since 2017, OmniVis has moved to South San Francisco, CA and grown to 8 full-time employees.

Location & Facilities

OmniVis is located in South San Francisco, CA at the ShangPharma Innovation coworking laboratory space.

We have several electronics stations, 2 3D printers, and craft cutter for thin layer rapid prototyping. We also have numerous materials for optics, electronics, and mechanical prototyping.

We have our own private BSL2 lab space. The space comes with access to shared equipment, external laboratory staff, and janitorial service 5 days per week. OmniVis owns laboratory equipment necessary for our work. We have a QuantStudio 3, PCR workstation, microwave, and gel boxes, hood for cell culture, a benchtop orbital shaker for growing bacterial cultures, lyophilizer, standard size and mini 4°C refrigerator and -20°C freezer.

Our own private office space sits 3-4 employees with desks, access to conference rooms, event space, kitchens, common spaces, and internet. We use Slack and Zoom for communication from working from home.

Management & Employees

OmniVis was founded by Drs. Katherine Clayton, Tamara Kinzer-Ursem, Jacqueline Linnes, and Steven Wereley as a University spin-out. Katherine works full-time at the CEO for OmniVis, where she sets vision, raises funds, and leads the team.

- Business Team: Our business team is managed by Michelle Florian, Finance Manager, and Lotte Vandewalle, Operations Manager. Michelle and Lotte lead timeline, daily operations, partnership relations, financial forecasting, budgeting, and grant management.
- Science Team: Our scientists, Nelda Vázquez-Portalatín, PhD, Senior Scientist, and Carlos Ponce-Rojas, PhD, Molecular Biologist, develop the assays and perform extensive scientific characterization for the OmniVis product. They also lead regulatory efforts with governing bodies like the FDA.
- Engineering Team: Global Health Engineer, Jordan Florian, Electrical Engineer, Juan Ayala, and Mechanical Engineer, Garry Valadez, bring their combined strengths together to develop our test kit and handheld device. Together they design, prototype, and work with manufacturers to bring our product to market.

Legal Structure

OmniVis is a Delaware C-Corp. We transitioned to a C-Corp on June 29, 2020 from a Limited Liability Company (from October 2, 2017 - June 29, 2020).



3. Market Analysis

Industry Analysis

Cholera exists in 51 countries and infects 3-5M people annually. The predominant players in the cholera ecosystem are those on the clinical response, water and sanitation, vaccination, and surveillance. There is demand to detect cholera before patient infection due to the cost to treat patients, the need for recurring chlorination and integration of WASH systems, and the underreporting of cholera cases and inaccurate surveillance. As cholera has not been eliminated and testing water is costly (\$125/test) and requires intricate laboratory infrastructure, there is demand for less expensive testing in low resource areas. Cholera outbreaks predominantly occur in the rainy season, indicating sales cycles for cholera test kits and treatment kits occur during wetter seasons. Additionally, vaccine penetration in cholera-ridden areas is low, therefore indicating the need for further testing in water resources for proactive approaches to eliminate disease spread. The Global Task Force for Cholera Control was created by multilateral agencies to reduce cholera by 90% by 2030.

Target Customers

OmniVis' customers are the procurement officials within humanitarian aid organizations, principal investigators within water testing facilities, and community leaders in regions where cholera is present. Though these individuals may not be the end-user of the physical device, the data the device generates is targeted towards them. There currently lacks a reliable method for collecting results and generating reports. Therefore, our data generation not only enables aid organizations to respond more quickly to the presence of cholera, but also provides quantitative information for performance and budget justification.

The users of our device are the field workers within each of these customer segments or laboratory technicians. The end beneficiaries of the OmniVis technology are the community members that may be affected by or vulnerable to cholera.

Competitors

There are two methods to diagnosis and detection methods recommended by the CDC: laboratory testing and Crystal VC Rapid Diagnostic Test. Laboratory testing provides accurate and reliable results; however, results may take up to a week, are costly, and require lab equipment and technicians. Laboratories are limited to 3-5 days, at the fastest, due to the time it takes for cholera cell enrichment, isolation, culture growth, PCR, and 2nd party verification via PCR. The Crystal VC RDT is affordable and provides rapid results, however this test is designed to diagnose patient stool samples not environmental samples. Neither have the ability to map or track hotspots and data.

Competitive Advantages

OmniVis has the speed of a rapid test with the accuracy of a laboratory test.

Table I. Competitive Matrix. The red-filled entries indicate that the product feature does not exist, while the green-filled entries indicate that the product feature does exist.

Name of Company	OmniVis	Crystal VC Dipstick	Lab Testing
Time of Test	30 minutes	20 minutes	3-7 days
Cost per Test	\$10	\$2	\$100
Accuracy	94.7%	65%	95%
Mapping System			
Environmental Test			

Regulations

For cholera, OmniVis will need to pursue WHO pre-qualification. While not required, stakeholders prefer WHO pre-qualification approval for dissemination of our product. The WHO pre-qualification process takes 1 year from submission to approval. We will work with Parexel as our liaison between the WHO and OmniVis due to their expertise in regulatory.



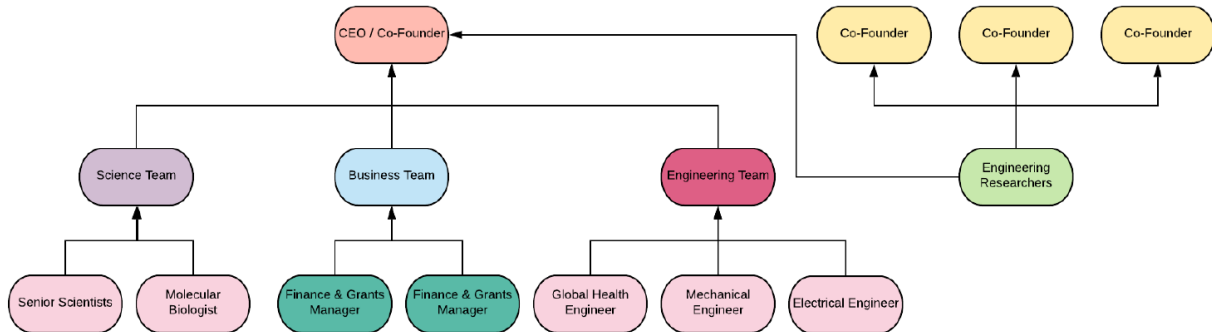
For patient-facing diseases in future years, OmniVis will submit to the FDA for a 510k. This regulatory process is necessary for non-invasive diagnostics (in vitro diagnostics). The process costs \$11,000 and takes 1-2 years from submission to approval. FDA approval requires bench testing, flex tests, and clinical trials. The process will allow us to legally sell our product in the United States and other countries where regulatory bodies may not be present, but would prefer FDA regulatory approval.



4. Organization & Management

Organizational Structure

We have four cofounders, a business team, science team, and engineering team. Our organizational chart can be seen below.



Ownership

Considering full diluted shares, Katherine Clayton owns 70% of OmniVis. Tamara Kinzer-Ursem, Steven Wereley, and Jacqueline Linnes equally own 5% of OmniVis. Finally, the employee equity pool is 15%.



5. Products & Services

Product & Service Benefits

Though primarily product focused, OmniVis is both a product and service company. Our initial product is a mobile-based cholera detection platform that combines (1) a hardware platform that serves as a mobile laboratory, (2) a disposable test kit used to collect water samples, and (3) software in the form of a mobile phone application. Upon product commercialization, we will provide software as a service (SaaS) to our customers, offering data visualization and reporting tools for disease outbreaks. As the first company to market a mobile water testing solution for cholera that also distributes results and data digitally, we expect to establish ourselves as the premier mobile cholera detection platform globally. To ensure our success, we have researched the market opportunity and market challenges extensively, as well as establishing partnerships that will best support us in successful deployment and integration into our target regions.

Pricing Structure

Our business model is similar to that of a razor-razorblade model with the hardware testing platform as the razor and disposable test chip as the razorblade. This strategy allows us to generate reliable and recurring income while locking customers onto our platform, building long-term relationships. As a one-time purchase, our hardware platform will be sold for \$1,000 (target 65% margin) with recurring income in the form of our disposable test kits at \$10 (target 80% margin) a piece. We will create supplemental revenue by rolling out a subscription model for our software once our product is on the market.

Lifecycle

The product lifecycle at OmniVis is initiated with product line ideation and customer discovery interviews and stakeholder analysis. From these interviews we determine product-market fit. Following, we design the product and iterate the device based on user feedback and field studies as well as cost to make. We then publish manuscripts and white papers on the scientific data to grow trust with customers.

We will introduce our first product, the handheld hardware and disposable test kit for cholera testing in water, in Q1 2022. We will focus on sales to small and medium sized water testing laboratories and then grow our customer base to larger NGOs and governments. Further, we will start with sales in Kenya and Bangladesh and grow our focus to other cholera endemic regions. With that we will also grow and scale manufacturing. Eventually, we will saturate the market for cholera testing organizations and need to produce new disposable test kits for other waterborne diseases and other pathogens in patients, food, and animals to grow our customer base and scale our company.

Intellectual Property Rights

The four founders of OmniVis submitted two pending patents while working full time for Purdue University. These patents are exclusively licensed by OmniVis through Purdue University. As exclusive licensees of the patent, we have freedom to operate and sub-license the technology anywhere in the world. We carefully protect future know how and technology by creating strict guidelines for every project we have with partners and contractors, enforced by NDAs and mutually agreed contracts. We have the support and weight of the Purdue Research Foundation and Bracewell LLP to protect the intellectual property associated with our technology.

1. System and methods for analyzing particles in a fluid. US10794808B2. Granted October 2, 2020.
2. Methods of measuring structural and functional changes of a biomolecular composition. Application US15/846,430.

Research & Development

OmniVis performs all of its own R&D with funding from SBIR grants through the USDA, National Science Foundation, National Institutes of Health, and National Institutes of Standards and Technology.

We previously performed R&D to develop the assay, lyophilization techniques, test kit design, hardware design, and packaging for the OmniVis device. However, we have handed off most of this R&D toward small batch manufacturing, where we are now testing for repeatability, accuracy, and stability of the



different test components. Likewise, we are funded to perform 400 field tests for cholera testing in Kenya and Bangladesh with major cholera partners through grant funding.

Additionally, we are performing new R&D for assistive devices for the cholera test. One product we are working on is a bacterial concentrator, where we can take large volumes of water and concentrate its content to make our testing even more sensitive than before.

Likewise, OmniVis is currently performing R&D for a HIV viral load test that would integrate into our hardware reader. This R&D approach would make our device a plug-and-play solution to begin testing for new diseases in new markets. Such an approach would make our device scalable.

Our R&D is headed by our engineering and science team. We use Scrum methods to approach our R&D and hit milestones in short sprints with focused team efforts.

Additionally, we are strategizing for all of our R&D to take place in house so we can apply for further patents and grow our IP portfolio.



6. Marketing & Sales

Market Description

There are 3-5M cases of cholera annually, occurring in 51 different countries. The cholera causing bacterium, *Vibrio cholerae*, causes 130,000 deaths each year and is found in water sources (drinking, bathing, public sources) and on shellfish and seafood products. The cholera clinical testing market is valued at \$197M in 2021 with a CAGR of 38%. However, the Global Task Force for Cholera Control believes that cholera efforts in water and clinical testing combined with surveillance is worth \$2B. Treating 1 case of cholera costs \$65.6 for both the patient and clinic. However, if left untreated, cholera leads to a 50% mortality rate. Additionally, cholera can live up to 4 weeks in stool, allowing the bacteria to spread easily in water sources and infect humans who come into contact with it. There are over 20 NGOs, 41 governments, numerous water testing laboratories and hospitals that are working on cholera efforts.

Value Proposition

The OmniVis solution provides value to our customers with solutions that are:

- Rapid: result within 30 minutes of data collection, which is 240x faster than the gold-standard
- Accurate: accuracy of 94.4% at environmentally relevant bacterial concentrations in water
- Cost effective: device costs \$1,000 for the hardware (1/2 start-up cost) and \$10 per test kit (1/10th the cost/test for cholera)
- Scalable: allows for detection of *V. cholerae* through viscosity measurements and has potential for use in other pathogen diagnostics (*S. aureus*, *K. pneumoniae*, *E. coli*, malaria)
- Portable: the device is easily maneuverable and can fit in someone's hand
- Automated: removes the training needed to interpret results
- Location specific: automates record keeping with real-time data aggregation for surveillance

Distribution Channels

OmniVis will first target larger aid organizations and governments with a central location to ship our products to. As our devices and test kits do not require cold chain transport, this approach lowers the complexity in logistics handling. However, as a small startup with limited capital, we lean on our customers to trickle down distribution within the areas that they work in different countries and regions worldwide.

Our devices will be transported from the manufacturing centers that our devices are made at. Therefore, the manufacturers will have the proper QA/QC to store these devices until they are distributed to the customers of interest. OmniVis will be in charge of handling the relationship with the manufacturer and the customer to fulfill orders and oversee movement of product.

Communication Strategy

Our short term goal is to access companies and communities that are interesting and engaged in cholera in the water and sanitation sector by providing brand recognition behind OmniVis. From performing ~300 customer discovery interviews we need to be highly active and engaged on social media platforms such as Facebook and Twitter to get engagement from relevant NGOs and testing organizations. Further, we are strategizing the dissemination of our field data in the form of white papers and manuscripts to prove that our products work in the field. Finally, another major strategy is to have boots-on-the-ground at WASH cluster meetings where there are numerous relevant stakeholders. This communication strategy provides a sense of trust by seeing representatives from organizations demonstrating their device in person to aid in customer buy in.

Sales Force

Sales are headed by Lotte Vandewalle and Katherine Clayton as we are a small startup that is prerevenue.

However, we plan to first hire a Chief Commercialization Officer with expertise in sales and commercialization strategy in the medtech sector to take over sales within the next 6 months. Following, the CCO would grow the sales and sales team to include further experienced individuals on the OmniVis team.



Sales Activities

OmniVis will follow a 4-step plan to approach market entry:

1. Research and development of the cholera testing platform
2. Field testing with strategic partners
3. Turn strategic partners into customers
4. Leverage initial customers to drive market expansion

This 4-step plan is used for expansion to other disease and pathogen testing as well. This approach is governed by funding, research and development of product and deployment and data collection. To effectively achieve market penetration, OmniVis will develop a good rapport with employees at food production agencies and with water/sanitation organizations, aid organizations, water testing labs, or governments.

Currently, we have partnered with icddr,b (the largest cholera hospital in the world), Code for Africa, and Emerging Pathogens Institute.

Growth Strategy

We will first grow our sales through the cholera testing market. We will initially sell to small-and-medium sized water testing laboratories in Kenya and Bangladesh. Following, we will grow our customer base in these regions and then focus on aid organizations that have intricate distribution networks in Kenya, Bangladesh, and other cholera endemic countries. Finally, after building trust with these laboratories, we will reach governments in cholera endemic regions to close the loop on cholera water-based testing.

After we have grown our cholera line and hit several markets, we will then develop single-use disposable test kits that are compatible with our hardware device for other waterborne diseases. Typhoid and E. coli are highly attractive. The E. coli test in water could lead us to more domestic markets in the United States where the bacteria causes issues today.

Following the water testing market, we will then develop patient-facing diagnostics, such as HIV viral load testing and strep testing. However, due to the regulatory and sales expertise being vastly different from the water testing market, we want to move into this after maturing in the water testing market internationally and domestically. Therefore, we would hire sales teams with expertise in patient testing and begin in the US where we can more easily reach customers and distribute our product. Afterwards, we would consider moving back to international markets due to our strong partnerships that were already built in the water space.

We see that our technology can be used for other sectors (food testing for listeria, animal testing for diseases like canine whooping cough) and that we could go into these markets in the far future to continue growth and scale into new markets.



7. Operations

Production

OmniVis performs all R&D activities at its South San Francisco, CA headquarters. However, test kits are manufactured by Hochuen Medical Ltd. in Shenzhen China. The assay for the test kits, lyophilization (freeze-drying), integration of the assay, and packaging are all performed in Minnesota, USA. For the hardware, we source parts from different suppliers throughout China and the United States and assemble the devices in-house. To date, we have performed small scale manufacturing of test kits (in the thousands) and hardware devices (in the tens).

As we scale, we will produce devices at an all-in-one facility that sources, builds, assembles, and tests the quality of each hardware and test kit.

Location

OmniVis performs R&D and business operations in South San Francisco, CA.

Reagents and chemistries for assays are purchased throughout the US. Packaging and storage are also performed in the US. Likewise, PCB boards and optical assembly are performed in the US.

Test kit production is sourced from China as well as hardware casings, electronics sourcing, lenses, lasers, raw packaging materials, and batteries.

Suppliers

- Reagents: New England Biosciences, Agilent, Thermo Fisher Scientific, Integrated DNA Technologies, GeneScript
- Lyophilization Services: BioLYPH Ltd.
- PCBs: Macrofab
- Optical Assemblies: Precision Microfab
- Test Kits: Hochuen Medical Ltd.
- Lasers: Dongguan Blueuniverse Laser
- Miscellaneous Components: McMaster-Carr, Amazon
- Power Supply: Sager Power Electronics
- Power switch: ShanPu
- Adhesive: 3M
- Cables: DigiKey
- Touch Display: Huayuan Display Control Technique
- Camera: Kai Lap Technology
- Lenses: Alibaba
- Battery: General Electronics Battery



8. Financials

Our plan to secure commercialization involves leveraging non-dilutive grant funding to de-risk our technology during the research and development phase and raising supplemental investor funds for manufacturing, sales and marketing, clinical validation, and patient usability studies.

Currently pre-revenue, we will initiate sales of the OmniVis cholera detection kit in Q1 2022 and move into other water testing markets (E. coli and typhoid) by the end of 2022. Our break-even point occurs in 2023, due in part to the advantage of OmniVis' plug-and-play platform, which allows our multiple product lines to drive down production costs and increase revenue margins. To date, OmniVis has raised \$3.16M in non dilutive grants and awards. To commercialize our cholera detection kit, we are raising an equity financing round of \$1.5M. This Seed round will carry us through WHO pre-qualification, FDA pre-submission, expansion of our team to include sales and marketing personnel, scale-up manufacturing, and commercialization of our cholera detection product. We project to earn \$2.2M in revenue in the first 12 months of sales.

In the next 1.5 years, we plan to sell our cholera detection kit, submit our product for WHO pre qualification, submit our FDA pre-application for clinical applications of our diagnostic device, and expand our product line to include diagnostics for other waterborne pathogens (SARS-CoV-2 in wastewater, E. coli, and typhoid). In 2023 OmniVis will raise a series A round of \$15M to enable us to grow our market and focus beyond waterborne testing to bloodborne testing. We already have preliminary data regarding bloodborne disease testing with our device (specifically HIV, malaria, dengue) and are assessing the market. With the series A round, we will be able to grow our company headcount and get the initial data on HIV bench testing to achieve a series B funding. The series B funding round will be used to manufacture devices tailored specifically for bloodborne testing (starting with HIV), progress toward FDA clinical trials, and further grow our company. After this round we will need to assess if we want OmniVis to be acquired or move further through financing rounds until eventually reaching an IPO. However, it is too premature to assess our exit strategy at such an early stage.



A. Income Statement

Assumptions: Currently pre-revenue, our 2021 income statement reflects how income from non-dilutive grants and awards are funding the research & development and business operations driving us towards commercialization. Of the \$3.16M in non-dilutive funding awarded since 2018, we will have received \$2,655,745 by the end of 2021. The remaining funds will be distributed in 2022 according to the respective payment schedule of each grant funder. We expect that the remaining ~\$500k in receivable grants will be combined with grants in the pipeline to total about \$1,944,071 in contributed income in 2022. We assume that as we continue to explore applications into new diseases of interest, we will consistently receive between \$4M and \$5M in contributed income from non-dilutive sources from 2023-2025.

OmniVis' earned income from revenue will drive team expansion and grow our operating expenses accordingly in future years. We expect that in 2022 as we launch our product, we will see a significant increase in Sales & Marketing expenses. In future years, we expect to continue growing our team of sales and marketing personnel to drive sales and increase revenue, allowing us to develop new product lines and expand our global reach.

Income Statement	<i>actuals</i> 2021	<i>forecast</i> 2022	<i>forecast</i> 2023	<i>forecast</i> 2024	<i>forecast</i> 2025
<i>Unit Sales</i>					
Hardware	-	1,262	3,348	4,443	6,875
Test Kit	-	67,967	2,072,701	3,689,810	5,947,961
Total Unit Sales	-	69,229	2,076,049	3,694,253	5,954,836
<i>Earned Income</i>					
Hardware	\$ -	\$ 1,326,350	\$ 3,425,855	\$ 4,583,965	\$ 7,181,185
Test Kit	\$ -	\$ 953,298	\$ 26,690,184	\$ 47,014,913	\$ 69,779,690
Total Earned Income	\$ -	\$ 2,279,648	\$ 30,116,039	\$ 51,598,878	\$ 76,960,875
<i>Cost of Goods Sold (COGS)</i>					
Hardware	\$ -	\$ 902,060	\$ 1,299,511	\$ 1,432,823	\$ 2,247,427
Test Kit	\$ -	\$ 678,165	\$ 13,006,200	\$ 19,845,685	\$ 27,695,248
Cost of Goods Sold	\$ -	\$ 1,580,225	\$ 14,305,711	\$ 21,278,508	\$ 29,942,675
Gross Margin	\$ -	\$ 699,423	\$ 15,810,328	\$ 30,320,369	\$ 47,018,200
<i>Gross Margin %</i>	<i>0.0%</i>	<i>30.7%</i>	<i>52.5%</i>	<i>58.8%</i>	<i>61.1%</i>
<i>Operating Expenses</i>					
Sales & Marketing	\$ 1,288	\$ 497,602	\$ 2,283,889	\$ 6,592,097	\$ 8,889,254
General & Administrative	\$ 774,210	\$ 1,480,027	\$ 2,729,768	\$ 6,393,923	\$ 7,803,593
Research & Development	\$ 620,296	\$ 1,872,417	\$ 3,716,638	\$ 5,382,885	\$ 6,693,035
Depreciation	\$ 3,917	\$ 32,089	\$ 91,474	\$ 148,033	\$ 214,163
Total Operating Expenses	\$ 1,399,711	\$ 3,882,134	\$ 8,821,770	\$ 18,516,937	\$ 23,600,048
Operating Income	\$ (1,399,711)	\$ (3,182,710)	\$ 6,988,559	\$ 11,803,432	\$ 23,418,155
<i>Operating margin</i>	<i>0.0%</i>	<i>-139.6%</i>	<i>23.2%</i>	<i>22.9%</i>	<i>30.4%</i>
Contributed Income	\$ 1,267,377	\$ 1,944,071	\$ 4,250,000	\$ 4,250,000	\$ 5,000,000
Net Income Before Taxes	\$ (132,334)	\$ (1,238,639)	\$ 11,238,559	\$ 16,053,432	\$ 28,418,155
Income Taxes	\$ -	\$ -	\$ 2,007,618	\$ 3,371,221	\$ 5,967,813
Net Income	\$ (132,334)	\$ (1,238,639)	\$ 9,230,941	\$ 12,682,211	\$ 22,450,342
<i>Tax Loss Carry Forward</i>					
Opening balance	\$ 307,501	\$ 439,835	\$ 1,678,474	\$ -	\$ -
Less carry forward applied	\$ -	\$ -	\$ (1,678,474)	\$ -	\$ -
Plus: carry forward generated	\$ 132,334	\$ 1,238,639	\$ -	\$ -	\$ -
Closing balance	\$ 439,835	\$ 1,678,474	\$ -	\$ -	\$ -



B. Cash Flow Statement

Assumptions: OmniVis will see a net change in cash of -\$29,885 in 2021, ending the year with a balance of \$277,616. We have receivable funds from our current grant funders, grants in the pipeline, and plans to raise \$2,995,000 in equity financing to carry us through 2022 and end the year with a balance of \$1.7M. We expect that 2023 will be a year of major growth for OmniVis as we bring new products to market in the water testing space and raise a Series A round of \$15M to move into the bloodborne disease testing market, for which we already have preliminary data. We plan to keep our cash on hand high enough to maintain between 12 and 18 months of runway as we expand our team each year.

Cash Flow Statement	actuals		forecast		forecast	
	2021	2022	2023	2024	2025	
Net income	\$ (132,334)	\$ (1,238,639)	\$ 9,298,789	\$ 12,682,211	\$ 22,450,342	
+ Depreciation	\$ 3,917	\$ 32,089	\$ 91,474	\$ 148,033	\$ 214,163	
Accounts receivable	\$ -	\$ (114,295)	\$ (1,395,633)	\$ (1,077,085)	\$ (1,271,574)	
Inventory	\$ -	\$ (129,881)	\$ (1,045,930)	\$ (573,107)	\$ (712,123)	
Other current assets	\$ -	\$ -	\$ -	\$ -	\$ -	
Accounts payable	\$ 6,722	\$ 15,726	\$ 72,596	\$ 68,498	\$ 56,496	
Other current liabilities	\$ -	\$ -	\$ -	\$ -	\$ -	
<i>Net cash from operations</i>	\$ (121,695)	\$ (1,435,001)	\$ 7,021,296	\$ 11,248,551	\$ 20,737,304	
Capital Expenditures	\$ (63,190)	\$ (126,285)	\$ (296,928)	\$ (282,792)	\$ (330,654)	
Other non-current	\$ -	\$ -	\$ -	\$ -	\$ -	
<i>Net cash from investments</i>	\$ (63,190)	\$ (126,285)	\$ (296,928)	\$ (282,792)	\$ (330,654)	
Debt	\$ -	\$ -	\$ -	\$ -	\$ -	
Equity	\$ 155,000	\$ 2,995,000	\$ 15,000,000	\$ -	\$ 30,000,000	
<i>Net cash from financing</i>	\$ 155,000	\$ 2,995,000	\$ 15,000,000	\$ -	\$ 30,000,000	
Net Change in Cash	\$ (29,885)	\$ 1,433,714	\$ 21,724,368	\$ 10,965,759	\$ 50,406,650	
Cash at beginning of period	\$ 307,501	\$ 277,616	\$ 1,711,330	\$ 23,435,698	\$ 34,401,458	
Cash at the end of period	\$ 277,616	\$ 1,711,330	\$ 23,435,698	\$ 34,401,458	\$ 84,808,107	



C. Break-Even Analysis

The break-even point occurs in 2023. We assume that the cost of goods sold for each unit of hardware is \$716.59 in 2022 (32.1% profit margin) but lowers to \$330.50 in 2025 (68.7% profit margin) as we scale up production numbers and drive down costs. We further assume that the cost of goods sold for each disposable test kit will start at \$8.44 (15.6% profit margin) in 2022 but decrease to \$4.46 by 2025 (55.4% profit margin). In 2023 the total units sold exceeds the break-even units so that we see an overall profit margin of 23.2%.

Break-Even Analysis

	2021	2022	2023	2024	2025
Total units sold	-	89,229	2,076,049	3,694,253	5,954,836
Total earned Income	\$ -	\$ 2,279,648	\$ 30,116,039	\$ 51,598,878	\$ 76,960,875
Total COGS	\$ -	\$ 1,580,225	\$ 14,305,711	\$ 21,278,508	\$ 29,942,675
Total Gross Margin	\$ -	\$ 699,423	\$ 15,810,328	\$ 30,320,369	\$ 47,018,200
Average Gross Margin per unit	- \$	10.10 \$	7.62 \$	8.21 \$	7.90
Total Operating Costs	\$ 1,628,835	\$ 3,850,045	\$ 8,730,295	\$ 18,368,905	\$ 23,385,882
Break-Even Units	-	381,075	1,146,372	2,238,079	2,961,812



D. Balance Sheet

Assumptions: As OmniVis grows from 2021-2025, the company's assets will see an increase from \$336,889 to \$91,737,910. We assume that expansion of the R&D team of laboratory scientists will drive the capitalization expenses due to the requirement of large equipment purchases. These tangible assets will include 3D printers, a lyophilizer, and BSC hoods which will allow us to prototype in-house, allowing us to iterate on designs with efficiency and precision. We assume that future funding rounds will (Seed in 2021-2022 and Series A in 2023) will drive company growth and allow us to scale manufacturing in order to drive down production costs and increase our profitability.

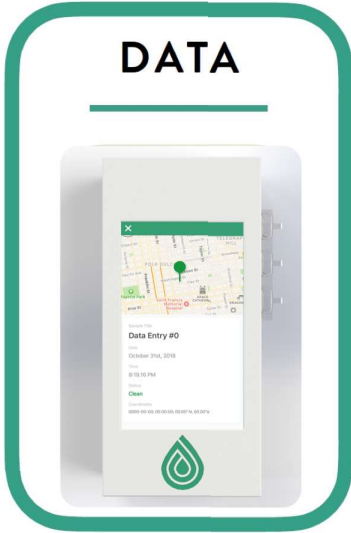
Balance Sheet	<i>actuals</i> 2020	<i>actuals</i> 2021	<i>forecast</i> 2022	<i>forecast</i> 2023	<i>forecast</i> 2024	<i>forecast</i> 2025
Cash	\$ 307,501	\$ 277,616	\$ 1,711,330	\$ 23,435,698	\$ 34,401,458	\$ 84,808,107
Accounts receivable	\$ -	\$ -	\$ 114,295	\$ 1,509,927	\$ 2,587,012	\$ 3,858,586
Inventory	\$ -	\$ -	\$ 129,881	\$ 1,175,812	\$ 1,748,918	\$ 2,461,042
Other current assets	\$ -	\$ -	\$ -	\$ -	\$ -	\$ -
Total Current Assets	\$ 277,616	\$ 1,955,506	\$ 26,121,438	\$ 38,737,388	\$ 91,127,736	
Tangible fixed assets	\$ 63,190	\$ 189,476	\$ 486,404	\$ 769,196	\$ 1,099,849	
Accumulated Depreciation	\$ (3,917)	\$ (36,006)	\$ (127,480)	\$ (275,512)	\$ (489,675)	
Net fixed assets	\$ 59,273	\$ 153,470	\$ 358,924	\$ 493,683	\$ 610,174	
Other non-current assets	\$ -	\$ -	\$ -	\$ -	\$ -	\$ -
Total Assets	\$ 336,889	\$ 2,108,976	\$ 26,480,362	\$ 39,231,072	\$ 91,737,910	
Accounts payable	\$ 6,722	\$ 22,448	\$ 95,044	\$ 163,543	\$ 220,039	
Other current liabilities	\$ -	\$ -	\$ -	\$ -	\$ -	\$ -
Total current liabilities	\$ 6,722	\$ 22,448	\$ 95,044	\$ 163,543	\$ 220,039	
Long-term debt	\$ -	\$ -	\$ -	\$ -	\$ -	\$ -
Equity	\$ 155,000	\$ 3,150,000	\$ 18,150,000	\$ 18,150,000	\$ 48,150,000	
Retained earnings	\$ 175,167	\$ (1,063,472)	\$ 8,235,317	\$ 20,917,528	\$ 43,367,871	
Total equity	\$ 330,167	\$ 2,086,528	\$ 26,385,317	\$ 39,067,528	\$ 91,517,871	
Total Liabilities and Equity	\$ 336,889	\$ 2,108,976	\$ 26,480,361	\$ 39,231,071	\$ 91,737,909	



9. Appendix



The OmniVis product.





US010794808B2

(12) **United States Patent**
Clayton et al.

(10) **Patent No.:** **US 10,794,808 B2**

(45) **Date of Patent:** **Oct. 6, 2020**

(54) **SYSTEM AND METHODS FOR ANALYZING PARTICLES IN A FLUID**

(71) Applicant: **Purdue Research Foundation**, West Lafayette, IN (US)

(72) Inventors: **Katherine Noel Clayton**, West Lafayette, IN (US); **Tamara Lea Kinzer-Ursem**, West Lafayette, IN (US); **Steven Truitt Wereley**, West Lafayette, IN (US); **Janelle Weslyn Salameh**, West Lafayette, IN (US)

(73) Assignee: **Purdue Research Foundation**, West Lafayette, IN (US)

(*) Notice: Subject to any disclaimer, the term of this patent is extended or adjusted under 35 U.S.C. 154(b) by 0 days.

(21) Appl. No.: **16/072,572**

(22) PCT Filed: **Feb. 3, 2017**

(86) PCT No.: **PCT/US2017/016414**

§ 371 (c)(1),

(2) Date: **Jul. 25, 2018**

(87) PCT Pub. No.: **WO2017/136664**

PCT Pub. Date: **Aug. 10, 2017**

(65) **Prior Publication Data**

US 2019/0072472 A1 Mar. 7, 2019

Related U.S. Application Data

(60) Provisional application No. 62/291,854, filed on Feb. 5, 2016.

(51) **Int. Cl.**

G01N 15/02 (2006.01)

G01N 15/00 (2006.01)

(52) **U.S. Cl.**

CPC . **G01N 15/0227** (2013.01); **G01N 2015/0038** (2013.01); **G01N 2015/0053** (2013.01); **G01N 2015/0238** (2013.01)

(58) **Field of Classification Search**

CPC **G01N 15/0227**; **G01N 15/0038**; **G01N 15/1463**; **G01N 15/10**; **G01N 2015/0053**; **G01N 2015/0038**

See application file for complete search history.

(56) **References Cited**

U.S. PATENT DOCUMENTS

2007/0229823 A1 10/2007 Sung et al.
2014/0231619 A1 8/2014 Yamaguchi et al.

OTHER PUBLICATIONS

Venu M. Gorti, "Immunoassays in Nanoliter Volume Reactors Using Fluorescent Particle Diffusionometry", Feb. 2, 2008, American Chemical Society (Year: 2008).*

(Continued)

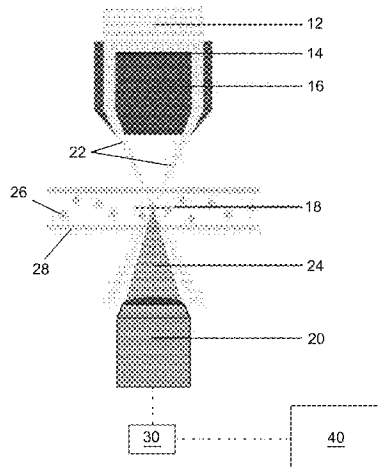
Primary Examiner — Maurice C Smith

(74) *Attorney, Agent, or Firm* — Hartman Global IP Law; Gary M. Hartman; Domenica N. S. Hartman

(57) **ABSTRACT**

Methods and systems suitable for tracking Brownian motion of particles suspended in a fluid and determining the diffusion coefficient of the particles therefrom in order to characterize the particles, their synthesis, and/or their surface modifications. The methods include providing a sample having particles suspended in a fluid, obtaining and recording at least first and second images of the sample wherein the first image obtained at a first time and the second image subsequently obtained at a second time, determining the average displacement of the particles in an area of the first and second images during a time period between the first time and the second time based on the first and second images, and then determining a diffusion coefficient of the particles in the area of the first and second images based on

(Continued)



the average displacement of the particles during the time period.

17 Claims, 9 Drawing Sheets

(56)

References Cited

OTHER PUBLICATIONS

Bob Carr, "Nanoparticle Tracking Analysis A Review of Applications and Usage 2010-2012", 2013 (Year: 2013).*

Sivaramakrishnan Ramadurai, "Influence of Hydrophobic Mismatch and Amino Acid Composition on the Lateral Diffusion of Transmembrane Peptides". 2010, Biophysical Journal vol. 99, p. 1452 (Year: 2010).*

International Search Report and Written Opinion dated May 12, 2017 for PCT/US2017/016414.

Detmer, Simon L. et al. "Local characterization of hindered Brownian motion by using digital video microscopy and 3D particle tracking"; Review of Scientific Instruments, 2014, vol. 85, No. 2, article No. 023708, internal pp. 1-10; see Abstract; internal p. 2, left column, line 39, right column, line 15 and figures 1-5.

Kumar, Alope et al., "Optical diffusometry techniques and applications in biological agent detection", Journal of Fluids Engineering, 2008, vol. 130, No. 11, article No. 11401, internal pp. 1-8, See internal pp. 1-4.

Modena, Mario M. et al., "Mass correlation spectroscopy for mass- and size-based nanoparticle characterization in fluid"; Journal of Applied Physics, 2015, vol. 118, No. 22, article No. 224901, internal pp. 1-11, See internal pp. 1-4.

Clayton, Katherine N. et al., "Physical characterization of nanoparticle size and surface modification using particle scattering diffusometry", Biomicrofluidics, Sep. 21, 2016 (e-pub), vol. 10, No. 5, article No. 054107, internal pp. 1-14; See internal pp. 2-12; and figures 1-5.

* cited by examiner

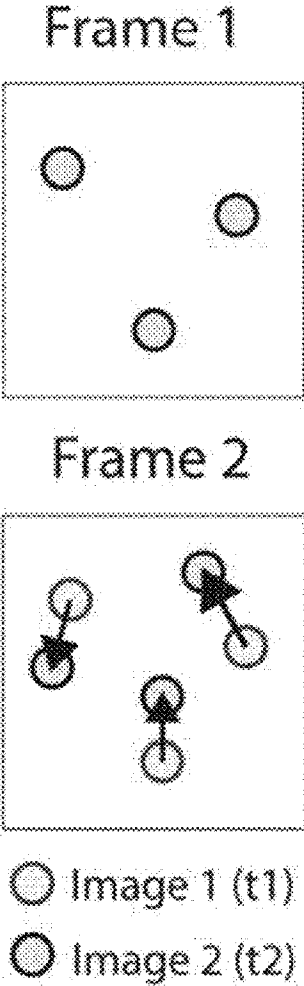


FIG. 1

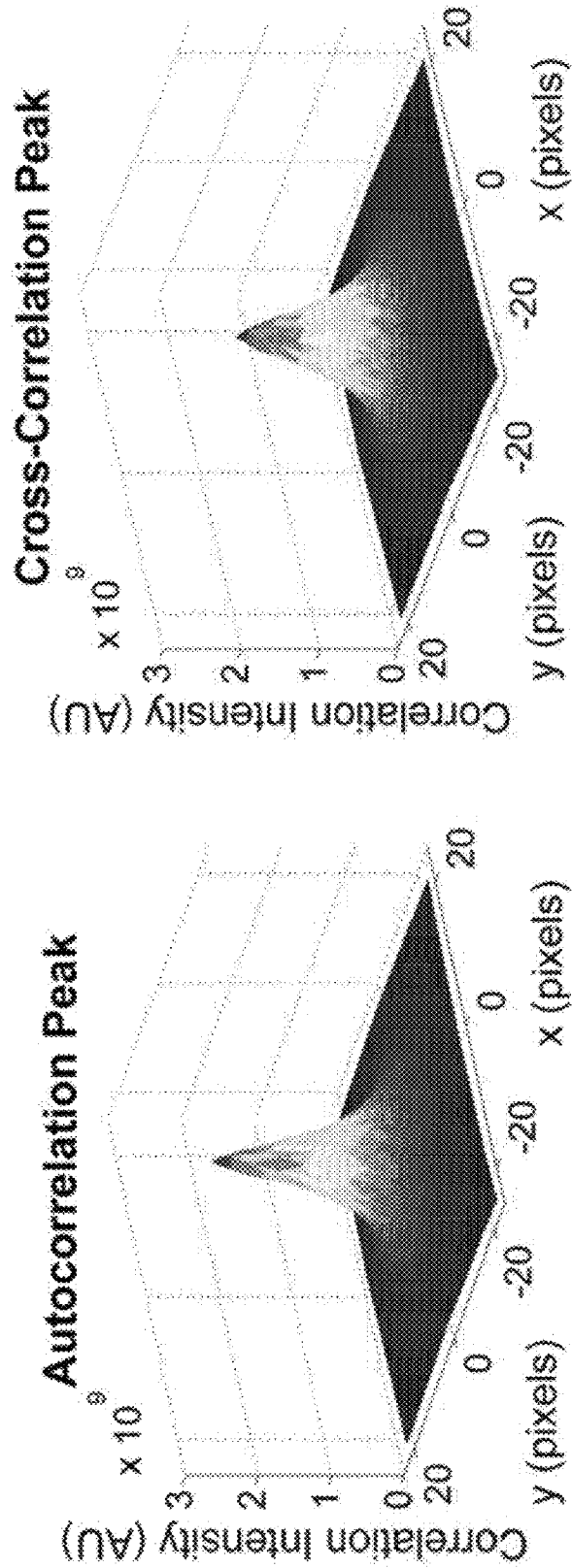


FIG. 2

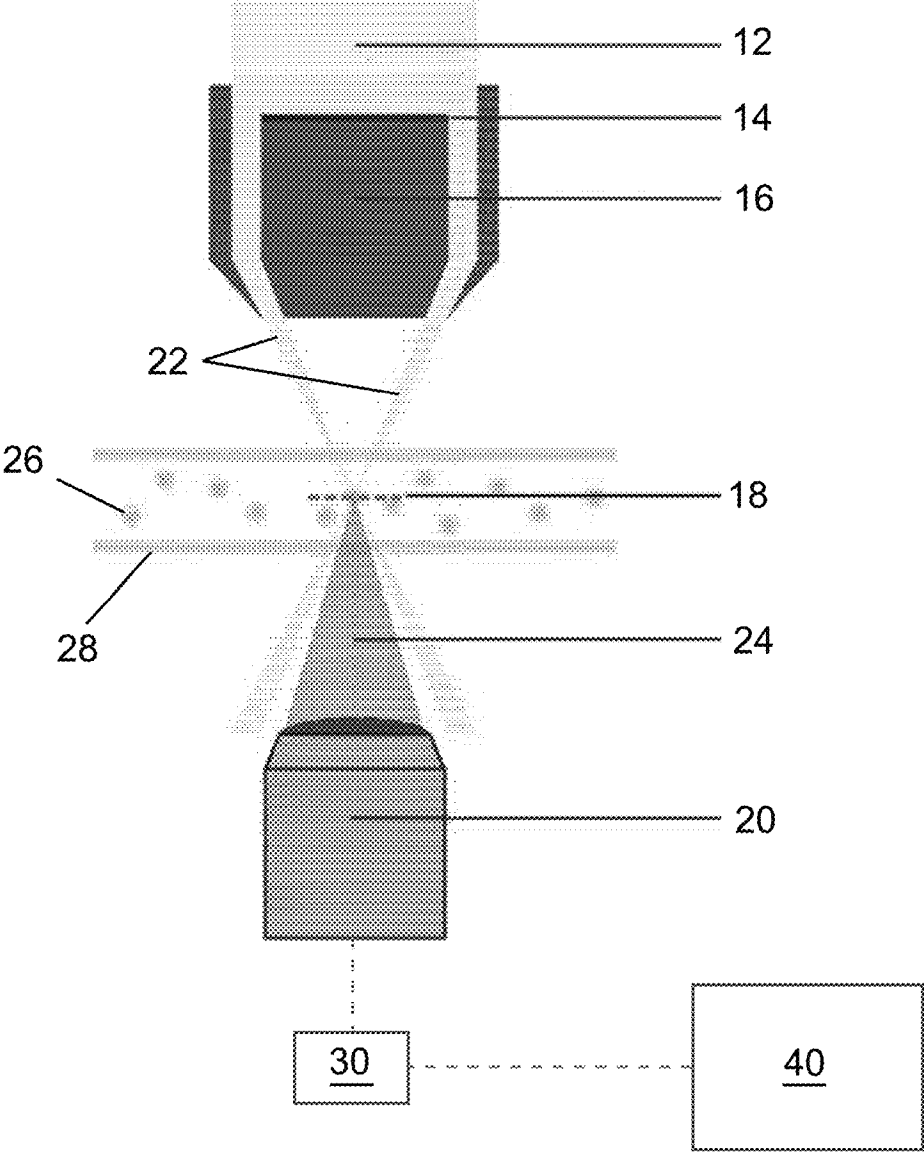


FIG. 3

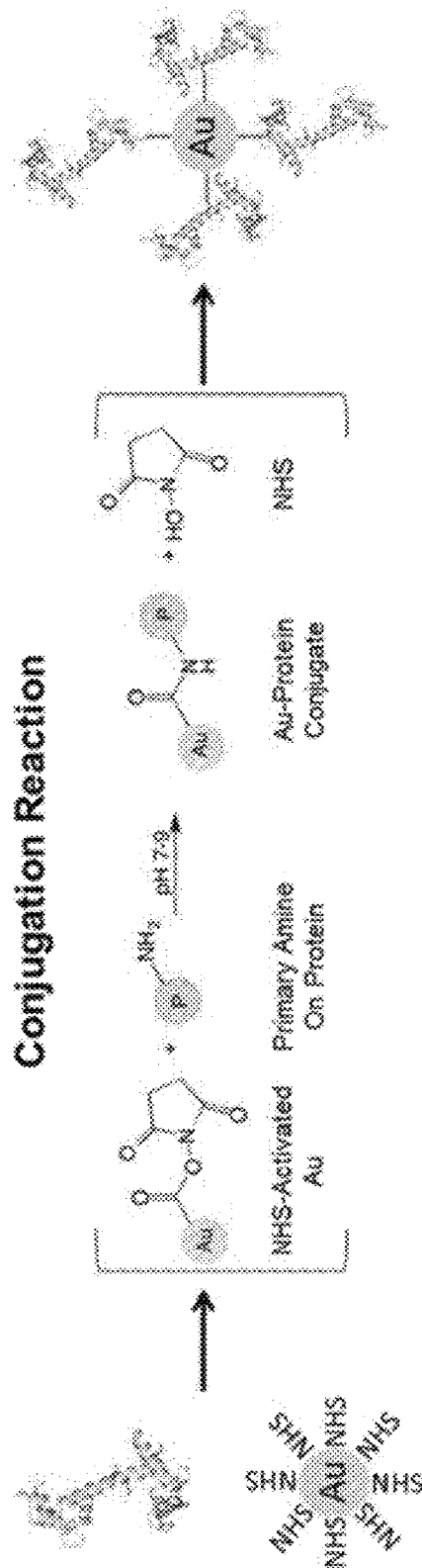
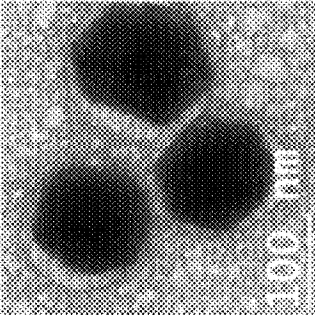
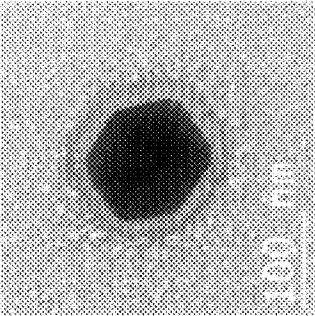


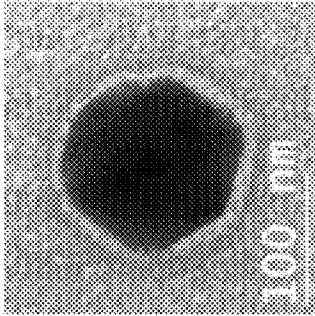
FIG. 4



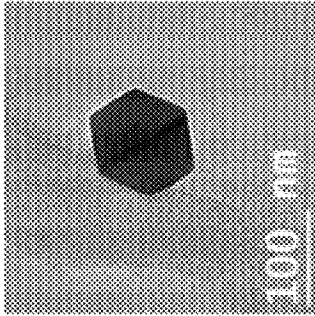
CaM



Lysozyme



BSA



Bare

FIG. 5

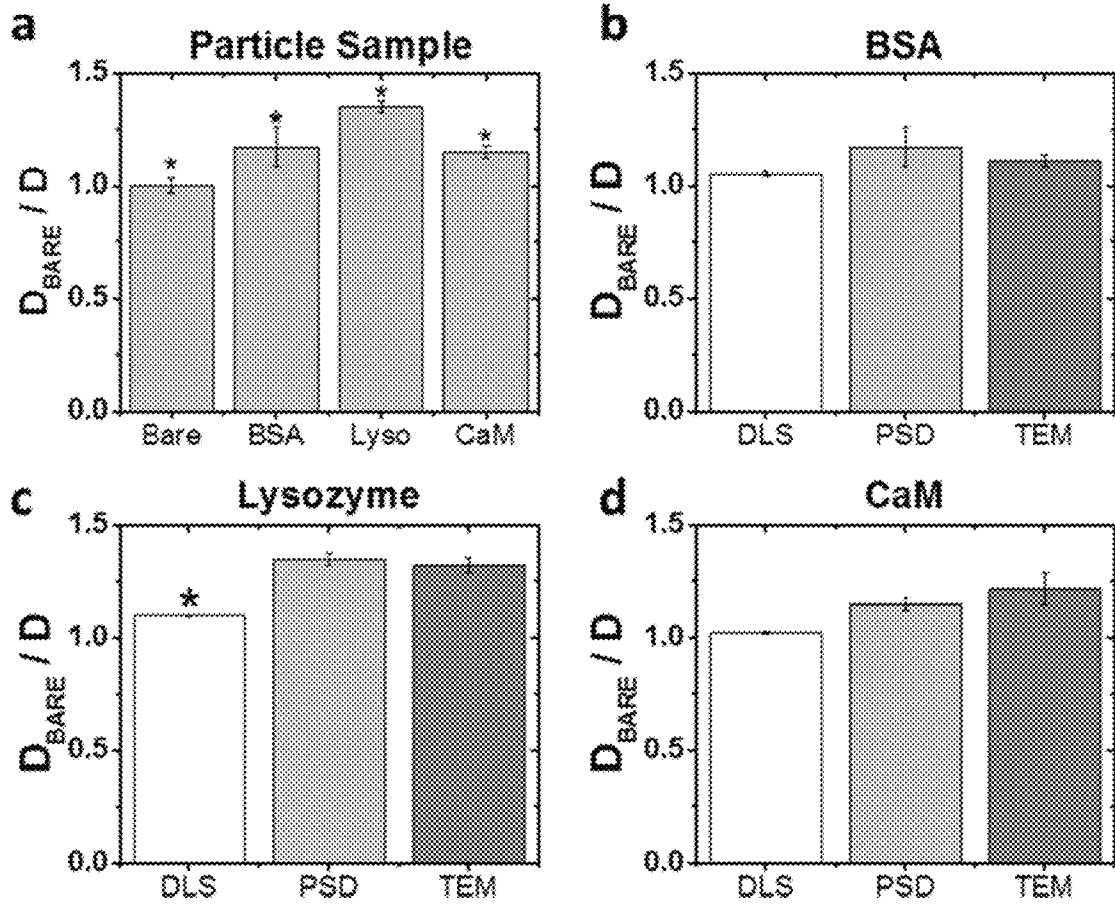


FIG. 6

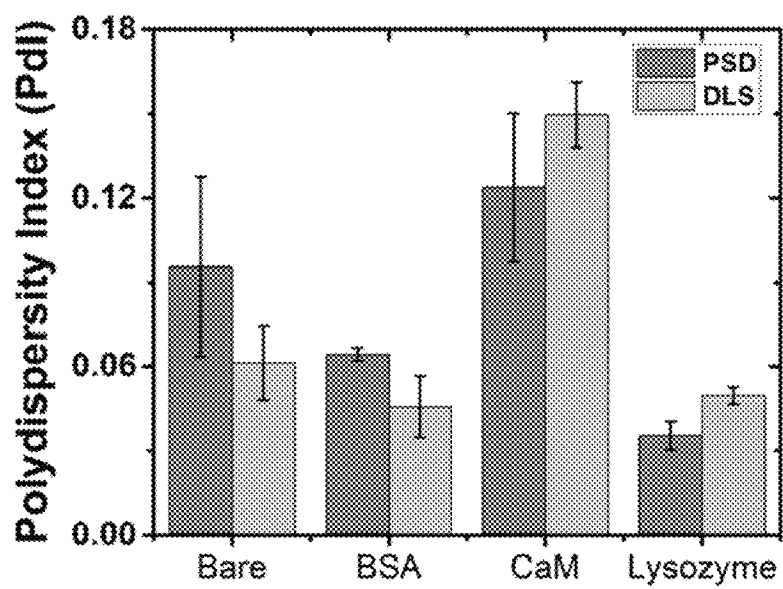


FIG. 7

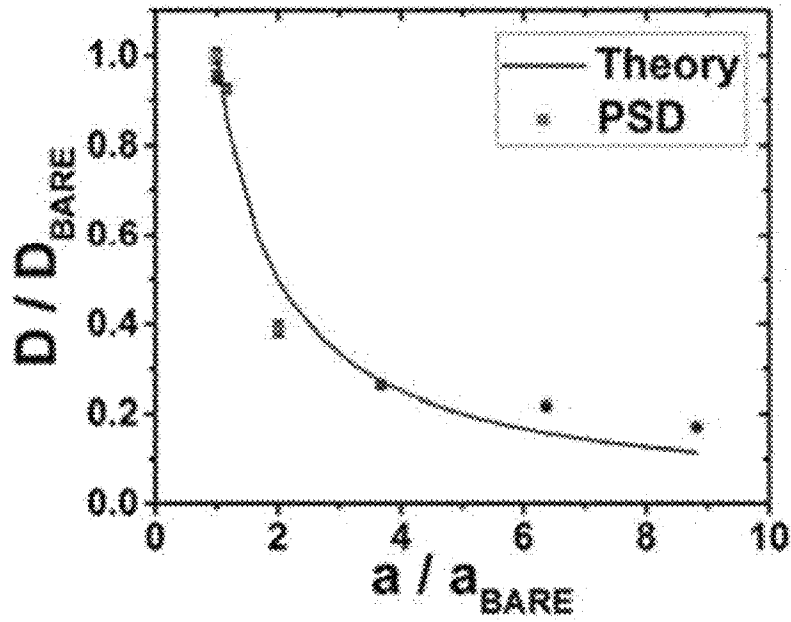


FIG. 8

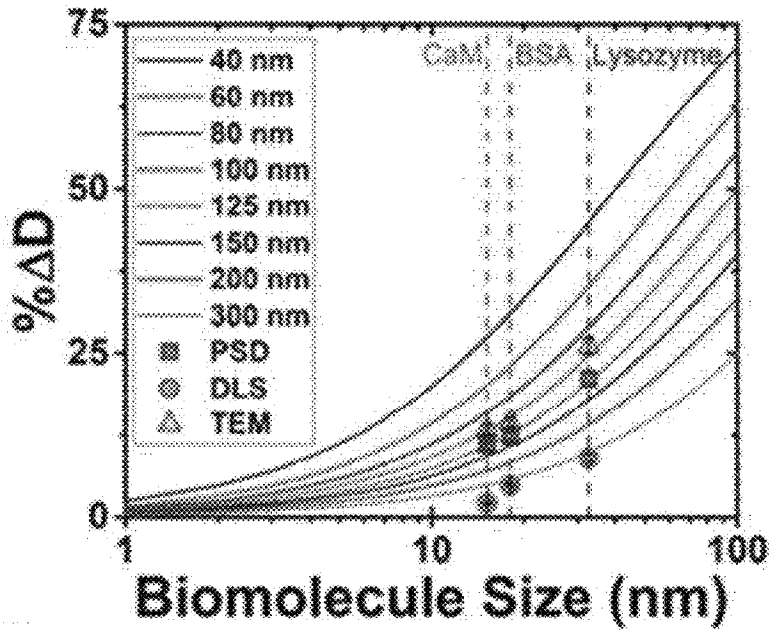


FIG. 9

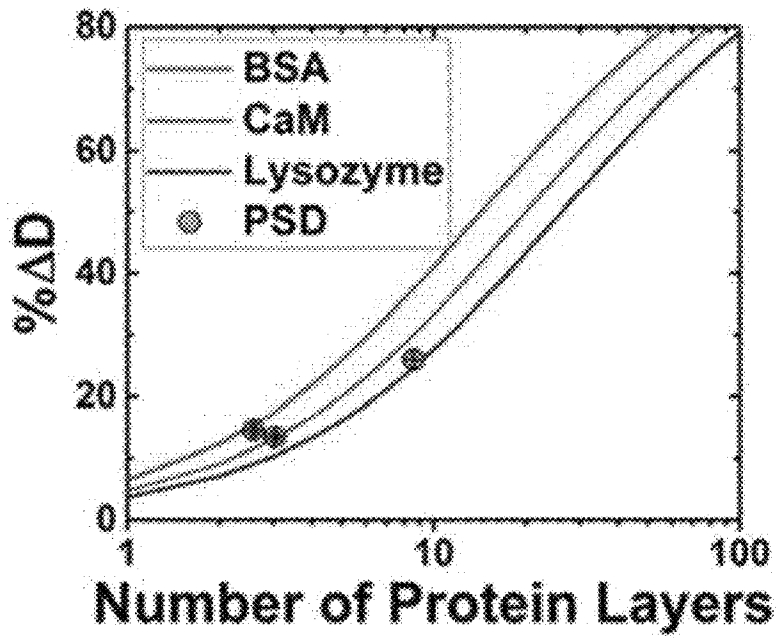


FIG. 10

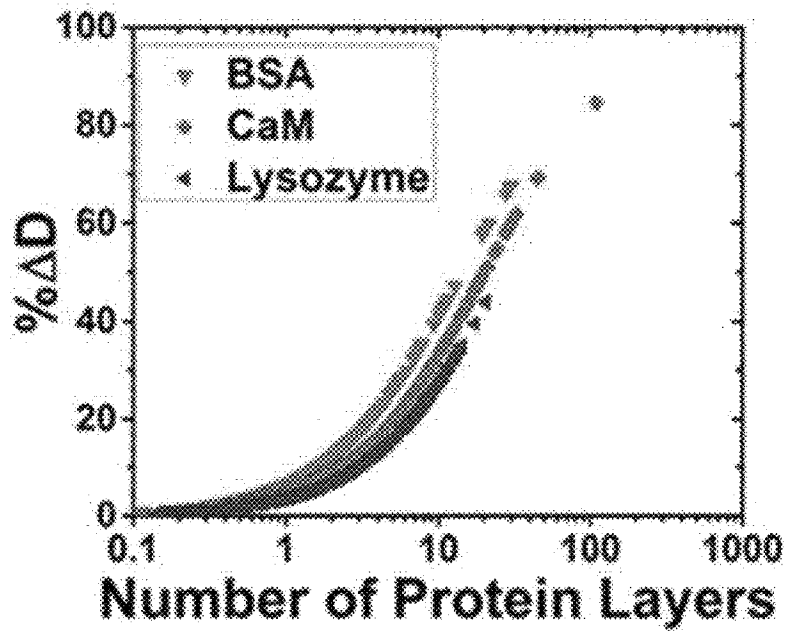


FIG. 11

SYSTEM AND METHODS FOR ANALYZING PARTICLES IN A FLUID

BACKGROUND OF THE INVENTION

The present invention generally relates to particle analysis. The invention particularly relates to imaging methods and systems for characterization of nanoparticles.

Current methods used to characterize nanoparticle synthesis and surface modifications include surface enhanced Raman spectroscopy, Fourier transform infrared spectroscopy (FTIR), electron microscopy, ultraviolet-visible spectroscopy (UV-Vis), and dynamic light scattering (DLS). Of these techniques, DLS is the most commonly used, measuring particles down to sub-nanometer sizes (e.g., less than one nanometer). This well-established method requires information from the user such as refractive index (RI), absorption coefficient, and properties of the fluid medium. This information is not always known a priori and surface modifications may, in fact, change some of these properties.

Notable examples of the use of nanoparticles (i.e., particles with a maximum dimension of less than one micrometer) in bio-nanotechnology include, but are not limited to, vehicles for nanomedicine, visual aids in point-of-care diagnostics, markers in immunohistochemistry, and detectors in biosensor design. In these exemplary applications, proteins that are conjugated onto nanoparticles can vary dramatically in size, from a Stokes radius of as small as 7 Å to as large as 1 and molecular weights from 10,000 Da to greater than 300,000 Da. Without a fluorescent label, it can be difficult to determine whether these biomolecules have been tethered to the particle surface, and nanoparticles formed of certain materials, such as gold, may quench fluorescence. Nonetheless, it may be important to characterize the addition of protein to nanoparticles, especially in applications where protein activity, proper structural folding, and catalysis are key factors. Thus, the development of practical tools for characterizing biomolecule conjugated nanoparticles would advance the bio-nanotechnology field into new application areas and provide improved quantitative measurements.

Accordingly, there is an ongoing desire for methods and systems capable of characterizing nanoparticles, as well as their synthesis and surface modifications.

BRIEF DESCRIPTION OF THE INVENTION

The present invention provides methods and systems suitable for tracking Brownian motion of particles suspended in a fluid and determining the diffusion coefficient of the particles therefrom in order to characterize the particles, their synthesis, and/or their surface modifications.

According to one aspect of the invention, a system is provided that includes an imaging device, means for recording a series of images of a fluid sample comprising particles suspended therein over a period of time, means for analyzing the series of images to determine an average displacement of the particles over the time period, and means for determining a diffusion coefficient of the particles based on the average displacement of the particles.

According to another aspect of the invention, a method is provided that includes providing a sample having particles suspended in a fluid, obtaining and recording at least first and second images of the sample wherein the first image is obtained at a first time (t_1) and the second image is subsequently obtained at a second time (t_2), determining the average displacement of the particles in an area of the first and second images during a time period (Δt) between the

first time (t_1) and the second time (t_2) based on the first and second images, and then determining a diffusion coefficient of the particles in the area of the first and second images based on the average displacement of the particles during the time period (Δt).

According to another aspect of the invention, a method is provided that includes providing a sample having particles suspended in a fluid, obtaining and recording a series of images of the sample over a period of time, partitioning each of the series of images into interrogation areas, determining the average displacement of the particles in each of the interrogation areas in each of the series of images over the time period, determining a diffusion coefficient of the particles in each of the interrogation areas in each of the series of images based on the average displacement of the particles, and then determining an average diffusion coefficient of the particles by averaging the diffusion coefficients in each of the interrogation areas in each of the series of images.

Technical effects of the methods and systems described above preferably include the ability to determine the diffusion coefficient of nanoparticles in a sample more accurately than conventional techniques, and without the need of certain foreknowledge about the sample (e.g., parameters such as refractive index (RI), absorption coefficient, and properties of the fluid medium).

Other aspects and advantages of this invention will be further appreciated from the following detailed description.

BRIEF DESCRIPTION OF THE DRAWINGS

FIG. 1 schematically represents sequential images (frames) showing nanoparticle Brownian motion during the time between frames 1 and 2. An analyzer can detect this change in the displacement of the nanoparticles in order to calculate the correlation in accordance with certain nonlimiting aspects of the present invention.

FIG. 2 schematically represents an autocorrelation peak (left) and a cross-correlation peak (right) of nanoparticles in a liquid as determined by particle diffusometry (PD). The autocorrelation peak is taller and narrower than the cross-correlation peak. The difference between the peak areas (along with magnification and time between images) provides the diffusion coefficient value.

FIG. 3 schematically represents a nonlimiting analyzer having a dark field attachment placed on an inverted microscope. A condenser blocks most light emitted by a white light source, focusing the emitted light to a small point within the specimen plane but outside the collection angle of the objective lens of the microscope. Only light scattered by the particles is collected by the objective lens of the microscope.

FIG. 4 schematically represents a nanoparticle protein conjugation reaction in accordance with investigations leading to nonlimiting aspects of the present invention. Proteins, in this case Calmodulin (CaM), are introduced to 100 nm N-Hydroxysuccinimide (NHS)-activated gold nanoparticles (AuNPs) where the NHS on the particle and primary amine on the protein react to form covalent protein-conjugated nanoparticles. This particular reaction conjugates onto any of the surface lysines on the protein.

FIG. 5 includes Transmission Electron Microscopy (TEM) images of bare (i.e., no protein), BSA (bovine serum albumin), lysozyme, and CaM conjugated AuNPs, respectively. The AuNP itself appears as the larger dark object in the image. The protein coated particles exhibit a halo-like feature around the particle circumference. This halo is the

conjugated protein, showing a minor change in contrast to the background of the image as compared to the AuNP. This is due to the fact that proteins are electron transparent.

FIG. 6 includes graphs representing comparisons of nanoparticle sizing techniques (DLS, PD, and TEM) performed on samples of BSA, lysozyme (“Lyso”), and CaM conjugated AuNPs. Image “a” compares the normalized diffusion ratios for the BSA, lysozyme, and CaM AuNP samples and a bare AuNP sample; PD shows a statistically significant ($p < 0.05$) detectable difference in the ratiometric diffusion coefficient (D_{bare}/D) between each sample of the four sample groups ($N=24$). Images b-d compare (D_{bare}/D) calculated from DLS, PD, and TEM data for the BSA, lysozyme, and CaM conjugated AuNPs, respectively.

FIG. 7 is a graph representing a comparison of the polydispersity index values between PD and DLS for bare, BSA (bovine serum albumin), CaM, and lysozyme conjugated AuNP samples. The difference in the polydispersity index between the two techniques is statistically insignificant ($p > 0.05$), indicating that PD can be used as a tool to determine sample uniformity.

FIG. 8 is a plot representing the ratiometric diffusion coefficients for particles of 100 nm, 300 nm, 520 nm, 1 μm , and 2 μm in diameter, and 100 nm biomolecule conjugated particles measured by PD and compared to the theoretical diffusion coefficient (Equation 2—represented as a line). The Root Mean Squared Error (RMSE) between theory and experiments was 6.04%.

FIG. 9 is a plot representing the percent change in the diffusion coefficient ($\% \Delta D$) theoretically determined for particles ranging from 40 nm to 300 nm in diameter as a function of the biomolecule size conjugated to the AuNP (represented as lines). The experimental data points (for the BSA, CaM, and lysozyme conjugated AuNPs) were calculated from TEM, PD, and DLS results and compared with theory. The dotted lines correspond to the thickness of the layer of each biomolecule as measured by TEM.

FIG. 10 is a plot representing the percent change in diffusion coefficient ($\% \Delta D$) as a function of the number of protein layers added to the 100 nm AuNP. Each protein’s Stokes radius changes the diffusion coefficient of the particle. The change in the diffusion for a bare particle compared to a protein conjugated particle allows to predict, on average, the number of layers of protein present on the particle using PD.

FIG. 11 is a plot representing diffusion coefficients experimentally determined for each separate interrogation area within an image frame. Based on the variation of diffusion coefficient measurements, the thickness of biomolecule layers on the AuNPs were predicted.

DETAILED DESCRIPTION OF THE INVENTION

The present invention generally provides methods and systems for performing image-based analysis of particles using particle diffusometry (PD). Imaging methods as described herein may be used to visually detect particles, calculate a diffusion coefficient of the particles, and therefore characterize small, label-free, biomolecular surface modifications. These processes include imaging particles over time, determining the Brownian movement of the particles during the observed time period, and then using this information to analyze the particles. These processes provide the ability to determine the size, uniformity, and/or biomolecule conjugation characterization of conjugated

nanoparticle solutions in smaller volumes and in less time than conventional techniques.

PD as disclosed herein involves measuring the diffusivity of particles undergoing Brownian motion. For example, particle motion in a fluid may be recorded with an imaging device, for example a camera, coupled to a microscope, over a predetermined time period and the recorded video (or series of images) of the particles may then be analyzed. During data analysis, each image (frame) of the recorded video may be partitioned into smaller areas (interrogation windows) such that, for example, on average eight to ten particles occupy each area. The average displacement of the particles within each area during the time between images may be determined using Fast Fourier Transforms (FFT), for example, with a Particle Image Velocimetry (PIV) computer software program.

Two different correlations are preferably computed using the FFT from which the diffusion coefficient may be extracted. A first of the correlations may be an autocorrelation, which is determined by correlating an area with itself. A second of the correlations may be a cross-correlation, calculated by correlating an area from a first image acquired at time t_1 with the same area from a second image acquired subsequently at time $t_2 = t_1 + \Delta t$, where Δt is the time between the consecutive first and second images (FIG. 1).

The correlation data may be fitted to a Gaussian distribution in order to measure the peak widths of both the auto- and cross-correlation data. The diffusion coefficient can then be calculated from the auto- and cross-correlation peak widths using the expression

$$D = \frac{s_c^2 - s_a^2}{16 M^2 \Delta t} \quad (1)$$

where the diffusion coefficient, D is determined from s_c and s_a , which are the auto- and cross-correlation peak widths measured at $1/e$ of the peak height (FIG. 2). M represents the magnification under which the particle images were recorded.

This fundamental equation was originally established in the context of PIV applications in order to understand how the velocity measurement uncertainty depended on temperature, but is applicable for PD to determine the diffusion coefficient of a species of particles. Because diffusion is essentially thermal noise, a large population of repeated measurements may be needed in order to accurately measure it. The diffusion coefficients calculated from each area in an image can be averaged together to produce a more precise measure of the diffusion coefficient. Averaging over more images can increase the precision still further.

PD is fundamentally different than other diffusion-based measurement techniques. In PD, unlike methods such as Nanoparticle Tracking Analysis (NTA), particles are analyzed in a continuum, meaning that individual trajectories are not calculated, but rather correlation is used to determine the difference in the displacement of many particles between image frames. This is known as an Eulerian approach. Because groups of particles are analyzed using correlation, PD is statistically robust. In contrast, NTA and the technique on which it is based, Particle Tracking Velocimetry (PTV), calculate particle size based on their trajectories in space. Multiple calculated particle trajectories are used to calculate the averaged mean squared displacement (MSD) curve, which is used to determine the diffusion coefficient. This is what is known as a Lagrangian approach.

5

The diffusion coefficient calculated from the particles' motion can be related to the fluid and particle parameters via the Stokes-Einstein equation,

$$D = \frac{kT}{6\pi\mu a} \quad (2)$$

where T is the absolute temperature, μ is the dynamic viscosity of the fluid medium, k is Boltzmann's constant, and a is the hydrodynamic radius. Combining these relationships, the particle hydrodynamic radius a is inversely proportional to diffusivity and hence to the area difference between the cross-correlation and autocorrelation peaks (multiply the numerator of Equation 1 by π). Thus, PD can be used to characterize properties that affect particle size as well as other fluid and particle parameters.

In addition to calculating the diffusion coefficient of a particle population, PD may also be used to measure the Polydispersity Index (Pdl) of the sample. Pdl is a parameter used to estimate the average uniformity of a particle solution. Larger Pdl values correspond to a larger size distribution in the particle sample and can indicate particle aggregation and/or the consistency and efficiency of particle surface additions throughout the particle sample. As used herein, a sample is considered monodisperse when the Pdl value is less than 0.1.

Particle Pdl may be measured by using PD to evaluate the particle Brownian motion in the areas in the series of images. Each area has its own auto-correlation and cross-correlation values, which are used to calculate the diffusion coefficient. Thus, each area in the image has a separate diffusion coefficient value. If each and every interrogation area exhibits a different diffusion coefficient, this indicates that there is also a relative difference in the particle's size. The greater the difference in the diffusion coefficient for each interrogation area, the larger the variety in particle size within the image. Based upon the Stokes-Einstein equation, the change in the particle's diffusion coefficient (D) is inversely related to its hydrodynamic radius. Each diffusion coefficient value may be plotted in a histogram and a normal distribution may then be fit to the data. From this fit, the Pdl can be calculated from

$$Pdl = \left(\frac{\sigma}{2a}\right)^2 \quad (3)$$

where σ is the standard deviation of the particle sizes measured in the normal distribution and a is the mean hydrodynamic radius.

PD analyzers are preferably capable of sizing particles and determining the uniformity of particle samples. Preferably, such analyzers are capable of analyzing particles having sizes (diameters or maximum dimension) of 20 μm or less, preferably nanoparticles having sizes of 100 nm or less, and more preferably between 100 nm and 30 nm or less. The lower limit in particle size depends on the sensitivity and fundamentals of the equipment used. For example, dark field and/or fluorescence microscopy are currently believed to be capable of analyzing particles as small as 30 nm suspended in fluid samples containing as little as one microliter of fluid. The upper limit of particle size is limited only by the ability of the particle to remain in solution over the time of the analysis, which is dependent on the density, size, and charge of the particle and not on the PD analyzer.

6

Consequently, PD analyzers may be capable of analyzing the size of particles over a relatively large range, for example, 20 μm to 30 nm. Such PD analyzers are believed to be more accurate in sizing nanoparticles than conventional techniques (e.g. Dynamic Light Scattering or Nanoparticles Tracking Analysis). These analyzers are believed to be beneficial not only for nanoparticle sizing but also for protein kinetics studies and bioassays. For such exemplary applications, the analyzers preferably are capable of analyzing particles as small as 30 nm, and measuring analyte modifications down to single protein layers.

A nonlimiting PD analyzer is schematically represented in FIG. 3 as comprising an inverted microscope having a dark field attachment and configured to image and analyze particles 26 suspended in a fluid medium within a fluid chamber 28. In this embodiment, the analyzer uses dark field imaging to allow a user to image particles 26 preferably as small as thirty nanometers in diameter or even smaller, depending on the sensitivity of a camera 30 coupled to the microscope. Using a dark-field attachment, the analyzer is capable of imaging and analyzing particles 26 having a size that is below the diffraction limit of the analyzer. A light stop 14 and condenser 16 of the dark field attachment blocks a majority of the white light source 12 of the microscope, allowing emitted light 22 to focus at a relatively small point within a plane 18 of fluid chamber 28, but outside the collection angle of the objective lens 20 of the microscope. As such, only light scattered 24 by particles 26 in the fluid chamber 28 is collected by the objective lens 20. Images captured by the camera 30 may be recorded and analyzed by, for example, a computer 40 functionally connected to the camera 30 and/or microscope.

The nonlimiting PD analyzer represented in FIG. 3 and described above uses dark-field microscopy to analyze particles 26 in the fluid chamber 28. Alternatively, a PD analyzer may include a fluorescence microscope and a camera to capture images of particles 26 suspended in the fluid chamber 28. Another embodiment may include a PD analyzer having a microscope (inverted or upright; no dark-field attachment) and a camera to capture images of particles 26 suspended in the fluid chamber 28. Yet another alternative embodiment may include PD analyzer having a camera to capture images of particles 26 suspended in the fluid chamber 28, wherein the particles 26 are large enough so that they are visible without microscopy.

In the setup represented in FIG. 3, the fluid chamber 26 may be configured to enclose various volumes of the fluid medium, for example, from less than several nanoliters to greater than several milliliters. In order for particle motion not to be hindered by the presence of a wall, the particles 26 are preferably imaged at least ten particle diameters away from any wall or edge of the fluid chamber 28. In practical terms, this means that the fluid chamber 28 is preferably structured with sufficient height and depth to allow imaging of particles 26 that are at least ten particle diameters from the walls of the fluid chamber 28. Generally, this is unlikely to be a limiting factor when considering nanoparticle size (i.e., less than one micrometer).

If the particles 26 are relatively small (about 200 nm in diameter or less), they are preferably formed of a material capable of scattering light suitably well in order to be visible. Therefore, metallic particles such as gold or silver are preferred for use with the analyzer. The concentration of these particles 26 may be optimized such that particle-particle interactions, which also hinder diffusion, are avoided but the particles 26 are still close enough together to capture many particles 26 in each image, reducing mea-

surement noise. This preferred particle concentration is determined so that, on average, particles **26** are located at least ten particle diameters away from one another. The fluid chamber **28** is preferably a closed system in order to minimize evaporation of the fluid medium and unintentional flow through the fluid chamber **28**. Evaporative effects may cause a net flow field that can disrupt PD measurements. Given these considerations, PD can be integrated at any stage within a micro- or nano-fluidic device where the particles **26** can be imaged.

Nonlimiting embodiments of the invention will now be described in reference to experimental investigations leading up to the invention.

In order to characterize biomolecule conjugation onto particles, several biologically relevant proteins (bovine serum albumin, lysozyme, and calmodulin) were covalently attached to gold nanoparticles (AuNPs). PD was used to measure the difference in Brownian motion between these samples compared to bare AuNPs. These proteins were chosen because they vary in size and charge from each other (Table 1) and are used in various biological applications. Bovine serum albumin (BSA) is a well-characterized blood serum protein that is commonly used as a blocking agent to minimize nonspecific protein interactions and nonspecific protein adsorption onto surfaces. Lysozyme is a hydrolase enzyme found in eukaryotes as part of the innate immune system. It is often used *in vitro* to break down bacterial cell walls and used widely in protein crystallography. Calmodulin (CaM) is a calcium ion (Ca^{2+}) binding protein found in all eukaryotic cells that modulates cellular responses to Ca^{2+} flux by binding and activating over 100 downstream target proteins. Calmodulin, along with green fluorescent protein, have been engineered to be intracellular Ca^{2+} biosensors.

TABLE 1

Properties of the proteins BSA, CaM, and lysozyme. The molecular weight (MW) and Stokes Radii show the range of protein sizes under study with PD. The isoelectric point (pI) relates to protein charge and the number of surface lysines indicate the number of locations where the protein may bind to the AuNP.				
Protein	MW (kDa)	Stokes Radius (nm)	pI	Number of Surface Lysines
BSA	66.50	3.48	4.7	30-35
Lysozyme	14.31	1.9	11.35	3
CaM	16.79	2.49	5.4	7-8

BSA, lysozyme, and CaM were separately covalently attached to N-Hydroxysuccinimide (NHS) functionalized gold nanoparticles (AuNPs) via primary amine chemistry as schematically outlined in FIG. 4. Protein conjugation was analyzed using Zeta potential analysis, Transmission Electron Microscopy (TEM), Dynamic Light Scattering (DLS), and PD. Measurements of nanoparticle Zeta potential and ratiometric diffusivity as determined by TEM, DLS, and PD, respectively, for bare, BSA, lysozyme, and CaM conjugated gold nanoparticles are summarized in Table 2 (below). Bare, BSA, Lysozyme and CaM conjugated particles had Zeta potentials of -6.37 ± 0.71 , -7.13 ± 0.71 , -10.11 ± 0.85 , and -12.03 ± 0.47 mV, respectively. This change in Zeta potential between the bare AuNP and the other three samples indicates protein attachment. TEM imaging showed that bare AuNPs have a hard and distinct edge whereas protein covered particles had blurred boundaries (FIG. 5). This blurring indicates that the proteins have successfully attached to the gold particle surface, as the blurring specifies a less electron dense material (i.e. the protein), as compared to gold. The

diameter of the bare AuNPs measured with TEM was 125.82 ± 2.359 nm. The protein layer thickness of each conjugated AuNP was 18.05 ± 3.191 nm for BSA, 32.69 ± 3.542 nm for lysozyme, and 15.16 ± 4.21 nm for CaM.

In order to determine the difference in the diffusion coefficient between the AuNP samples using PD, the ratio of the diffusion coefficient of bare AuNPs to the diffusion coefficient of protein conjugated-AuNP samples was calculated as a diffusion ratio (D_{bare}/D). The diffusion ratio is the value of the average diffusion coefficient of the protein-conjugated AuNPs relative to the diffusion coefficient of the bare AuNP. The ratio of the diffusion coefficients of two particle species in solutions of identical temperature and viscosity is inversely proportional to the ratio of their particle sizes:

$$\frac{D_{AuNP}}{D_{protein_AuNP}} = \frac{a_{protein_AuNP}}{a_{AuNP}} \quad (4)$$

where $D_{protein_AuNP}$ and $a_{protein_AuNP}$ are the diffusion coefficient and hydrodynamic radius of the protein conjugated particle and D_{AuNP} and a_{AuNP} are those of the bare AuNPs (also referred to herein as D_{bare} and a_{bare}). From this equation, it is apparent that as particle size increases due to biomolecular conjugation the diffusion coefficient of the conjugated particles decreases.

Representing the diffusion coefficient of the biomolecular conjugated nanoparticles as a ratio presents a distinct advantage of measuring these changes with shorter time measurements. When PD is used to find the time-averaged diffusion coefficient, a large number of images must generally be recorded in order to be accurate. Accuracy in this instance is defined as being within 2% of the theoretical diffusion coefficient value (as described by the Stokes-Einstein equation, Eq. 2). Although a large image set does reduce experimental error, measurements of absolute diffusion coefficients can take 20 minutes or longer because of the need for a large number of images. When using the diffusion coefficient ratio (D_{bare}/D), fewer images (frames) are needed to produce experimental error of the same scale as those of the absolute diffusion coefficient. Therefore accurate measurements of the radiometric diffusion can be performed in much shorter times.

For example, the absolute diffusion coefficient and error of 100 nm AuNPs was measured using 100 frames and using 10,000 frames, respectively. A t-test comparing the two errors showed that they were statistically different ($p < 0.05$), indicating that 100 frames was not sufficient to produce an accurate measurement. In contrast, a t-test comparing the error from the ratiometric approach using 100 images (about 8 seconds of data) and the error of the absolute diffusion coefficient using 10,000 frames was found to not be statistically different ($p > 0.05$). Therefore, it is possible to take advantage of the similarity in the scaled error to reduce the number of images and the overall measurement time.

The ratiometric diffusion coefficients of the conjugated BSA, lysozyme, CaM, and bare AuNPs were calculated with PD in order to demonstrate that the technique can be sensitive enough to detect a significant difference between the samples. PD measurements were compared to DLS and TEM measurements (Table 2). Using this technique, a statistically significant difference ($p < 0.05$) in the ratiometric diffusion coefficient between the bare, CaM, BSA, and lysozyme coated AuNPs (image a of FIG. 6) was determined. For example, lysozyme AuNPs gave the biggest

change in diffusivity which correlates well with the change in particle size measured via TEM. On the other hand, CaM conjugated AuNPs have the smallest change in the PD measured diffusion coefficient. PD was sensitive enough to measure a difference between all four particle samples with statistical significance.

In order to validate the accuracy of the PD method, the normalized diffusion ratio determined by PD was compared to TEM and DLS data for each protein-conjugated sample (images b-d of FIG. 6). In all cases (CaM, lysozyme, and BSA), there was no statistically significant difference between the TEM and PD measurement systems ($p > 0.05$) (images b-d of FIG. 6). In contrast, DLS measurements often exhibited lower ratiometric values as compared to TEM and PD, with a statistically significant difference in measurements for the lysozyme conjugated particles (image c of FIG. 6). Additionally, PD values were found to be consistently closer to the TEM data in comparison to DLS measurements. The difference between DLS and TEM for lysozyme, BSA, and CaM were 16.67%, 5.41%, and 16.02%, respectively whereas the difference between the TEM and PD was 2.27% (lysozyme), 5.41% (BSA), and 5.57% (CaM).

It was demonstrated that PD can predict the uniformity of a nanoparticle solution using Polydispersity Index (PDI) as an indicator. Polydispersity characterization is a factor in nanoparticle applications, as it is difficult to control sample-wide uniformity with surface conjugation chemistry, and often aggregation of particles can occur. Currently, DLS is the most common PDI measurement method.

To calculate sample PDI using PD, 100 images per data set were partitioned into areas (interrogation windows). Diffusion coefficient values were calculated from the nanoparticles within each area, and the array of values were fit to a normal distribution. A normal distribution was chosen in order to directly compare the PDI measurements with DLS, which also uses a normal distribution in its model. The PDI of the normal distribution was calculated according to Equation 3. PDI measurements for both PD and DLS are given in Table 3 (below) and shown graphically in FIG. 7. It was determined that there was no statistically significant difference between the PDI values measured using PD and DLS ($p > 0.05$). Both techniques determined that CaM conjugated nanoparticles showed the least uniformity between the samples with PDI values of 0.12-0.15, indicating that this sample was polydisperse (FIG. 7 and Table 3). Conversely, lysozyme coupled AuNPs displayed the highest degree of uniformity with PDI values of 0.035-0.05, indicating this sample was monodisperse (FIG. 7 and Table 3).

In order to compare experimental measurements of nanoparticle diffusion by PD to calculations of the diffusion coefficient by the Stokes-Einstein equation (Equation 2), the diffusion coefficients of bare particles with diameters of 100 nm, 300 nm, 520 nm, 1 μm , and 2 μm , and 100 nm particles conjugated to CaM, lysozyme, and BSA were measured using PD. For each case, the ratiometric diffusion was calculated as described above in Equation 4. As predicted, the ratiometric value measured by PD decreased as the particle's hydrodynamic radius (a in Equation 1) increased (FIG. 8). The values of the ratiometric diffusion coefficients for these particles are presented in Tables 2 and 4. The Root Mean Squared Error (RMSE) between PD data and Stokes-Einstein predictions was found to be 6.04%. This small RMSE indicates that PD can be used to determine the diffusion coefficient for a large range of particle sizes, extending beyond the nano-regime.

In order to determine the expected percent change in the diffusion coefficient, PD was used to calculate the average thickness of biomolecules bound to the nanoparticles and compared to predictions by the Stokes-Einstein equation (Equation 1). To identify how the diffusion coefficient of nanoparticles would change upon conjugation of biomolecules to the nanoparticle surface, the percent change in diffusion coefficient of various nanoparticles ranging in diameter from 40-300 nm was predicted as greater amounts of biomolecules increased the hydrodynamic radius of the particles (a function of the thickness of the biomolecules layering onto the surface during conjugation). A relationship between biomolecule thickness/layering and the nanoparticle hydrodynamic radius may be defined as:

$$\text{thickness}_{(\text{biomolecule_layer})} = a_{\text{total}} - a_{\text{bare}} \quad (5)$$

Further, the percent change in diffusion coefficient may be calculated using:

$$\% \Delta D = \frac{D_{\text{AuNP}} - D_{\text{protein_AuNP}}}{D_{\text{AuNP}}} \cdot 100 \quad (6)$$

The solid lines in FIG. 9 predict how the diffusion coefficient of particles, ranging from 40 nm to 300 nm in diameter, would change as a function of the size of the thickness of the biomolecule layer(s) bound to the particle surface.

Different nanoparticle characterization methods (TEM, DLS, and PD) were used to measure the percent change of the diffusion coefficient of protein conjugated nanoparticles (FIG. 9) in order to compare these methods to predictions from Equation 6 and observe how the relative consistency of the methods. TEM was used to directly measure the size of nanoparticles before and after biomolecule conjugation and percent change in diffusion coefficient was calculated according to Equation 7.

$$\% \Delta D = \frac{1/a_{\text{AuNP}} - 1/a_{\text{protein_AuNP}}}{1/a_{\text{AuNP}}} \cdot 100 \quad (7)$$

The diffusion coefficient of bare and biomolecule conjugated 100 nm AuNP was measured using PD and DLS. The percent change in the diffusion coefficient was calculated using Equation 6. Within each characterization method lysozyme conjugated AuNPs consistently had the largest percent change in diffusion coefficient followed by CaM, and then BSA with the smallest percent change in diffusion coefficient (FIG. 9).

In order to compare the accuracy measurement methods, the measured change in percent diffusion (dots in FIG. 9, values in Table 5 below) was compared to the predictions of the percent change in diffusion (solid lines in FIG. 9). It was seen that the change in the diffusion coefficient measured for the different biomolecules by TEM fell along the 100 nm predicted curve while PD fell along the 125 nm curve and DLS fell along the 300 nm curve. Because the particle's true size is about 100 nm in diameter, this TEM result matched well with predictions. In contrast to TEM, which is a direct measurement of size, PD and DLS estimate particle hydrodynamic radius. Thus it is not surprising that the PD measurement falls along the 125 nm curve as the nanoparticle's effective hydrodynamic diameter is different due to an electric dipole layer that forms about the particle's surface. In contrast, the DLS data was closest to the 300 nm curve. This indicates a larger inaccuracy in measuring the change

in diffusion coefficient as a function of different size biomolecule additions. Although DLS also measured the hydrodynamic radii, baseline DLS measurements of the bare 100 nm AuNPs remained at about 125 nm in diameter. Therefore the percent change in the diffusion coefficient based on DLS measurements indicate inaccuracies in the measurement system. These discrepancies can be attributed to two factors, a) the assumption in DLS that the particles in solution are spherical and b) as more biomolecule is added to the nanoparticle, the refractive index properties of the solution change. Given that DLS is an intensity-based measurement system, these factors can induce errors to the true particle size.

Characterizing the number of layers present on a nanoparticle is desirable for researchers performing layer-by-layer assemblies such as designing tunable vehicles for drug delivery devices. By coupling the Stokes-Einstein equation (Equation 2) and the biomolecule Stokes radius (Table 1) with PD measurements (Table 2) the average number of layers of protein that are conjugated to the nanoparticles may be estimated. The diffusion coefficient measured with PD is substituted into the Stokes-Einstein equation, calculating the overall thickness of the protein layer, as follows:

$$\% \Delta D = \left(\frac{n(a_{protein})}{a_{AuNP} + n(a_{protein})} \right) \quad (8)$$

where n is the number of protein layers attached to the particle. In FIG. 10, there are three theoretical curves that demonstrate how the change in the diffusion coefficient (calculated using Equation 6) allows for the estimation of the number of layers of protein (CaM, lysozyme, and BSA) that are conjugated on a 125 nm AuNP. Applying the Stokes radii ($a_{protein}$) of lysozyme, BSA, and CaM (found in Table 1), this change was predicted with Equation 8. Initially, the percent change in the diffusion coefficient was calculated from PD measurements (Equation 6) and this calculation was used to estimate the average number of protein layers, n , that were conjugated to the AuNP surface (FIG. 10, dots). The lysozyme conjugated particles have the largest number of layers on the AuNP surface whereas the BSA had the least amount. This agrees with TEM measurements and can be seen in FIG. 5.

In addition to estimating the average number of protein layers on the nanoparticles, one may characterize the variation in the number of protein layers throughout the nanoparticle sample. For example, with antibody coated nanoparticles used for drug therapy, it may be important to know how much of the therapeutic is attached to the particle surface. Particles with varying layers throughout the sample or particles with a large number of layers may see effects in affinity, functionality, and steric hindrance. Therefore, a method to use PD measurements was established to estimate the variation in the protein layering within the sample. In a set of images, each area (interrogation window) may exhibit a different diffusion coefficient value. The range of these diffusion coefficient values may be used to calculate the variation in the number of biomolecule layers of a particle sample. The percent change of the diffusion coefficient (Equation 6) for each area (keeping D_{AuNP} constant at $3.56E-12 \text{ m}^2/\text{s}$) may be calculated and Equation 8 may be used to calculate the number of protein layers per area. The results for the variation of biomolecule layers for each sample (lysozyme, CaM, and BSA) are plotted in FIG. 11 where every point represents a measurement in a single area.

If a protein conjugated nanoparticle sample is more uniform, then there will be less distribution of points along the x-axis. This is because each of the areas would have a similar diffusion coefficient to one another. With data presented in this way one can visualize the distribution of the number of protein layers within a sample to compliment the PDI measurement. For example, lysozyme conjugated nanoparticles had the smallest distribution along the x-axis, indicating that the surface coating was more uniform throughout the sample. This agrees with the PDI measurement of the lysozyme particles (PDI=0.049). In contrast, the CaM modified AuNPs, had the largest distribution of number of protein layers which is in agreement with the large PDI value (0.124). In the samples, it was observed that clusters of CaM-conjugated nanoparticle samples had predicted layers of 100 and 200 layers, indicating aggregation. Visualizing the distribution of the number of protein layers in this way may be a useful technique to discern nanoparticle aggregation versus a continuous distribution of nanoparticle sizes. These differences might not be seen by visual inspection of a sample, nor by PDI measurement, but can be readily discerned by estimating the distribution of the number of protein layers.

TABLE 2

Ratiometric diffusion coefficients ($D_{AuNP}/D_{protein-AuNP}$) of TEM, DLS, and PD measurements of protein conjugated gold nanoparticles and their corresponding Zeta Potential values.

Sample	TEM	DLS	PD	Zeta Potential (mV)
BSA	1.22 ± 0.071	1.05 ± 0.009	1.17 ± 0.091	-7.13 ± 0.71
Lysozyme	1.32 ± 0.033	1.10 ± 0.002	1.35 ± 0.025	-10.11 ± 0.85
CaM	1.11 ± 0.026	1.02 ± 0.004	1.15 ± 0.026	-12.03 ± 0.47

TABLE 3

DLS and PD Polydispersity Index (PDI) measurements for bare, BSA, CaM, and lysozyme conjugated AuNPs.

Sample	PD PDI	DLS PDI
Bare AuNP	0.0956 ± 0.03193	0.0613 ± 0.01313
BSA AuNP	0.0645 ± 0.00238	0.0457 ± 0.01091
CaM AuNP	0.1238 ± 0.02639	0.1497 ± 0.01157
Lysozyme AuNP	0.0354 ± 0.00516	0.0496 ± 0.00287

TABLE 4

Inverse ratiometric diffusion coefficient of polystyrene particles (D/D_{bare}) from 300 to 2000 nm in diameter measured experimentally by PD as well as their predicted value using the Stokes-Einstein equation.

Sample	Prediction	PD
300 nm	0.4960	0.389 ± 0.017
520 nm	0.2714	0.264 ± 0.006
1000 nm	0.1569	0.218 ± 0.003
2000 nm	0.1134	0.170 ± 0.002

Note that the ratiometric diffusion coefficient in this table is calculated as D/D_{bare} to reflect the inverse relationship between particle size and diffusion coefficient.

TABLE 5

Percent change in diffusion (% ΔD) determined by TEM, PD, and DLS measurements			
Sample	TEM	PD	DLS
Lysozyme	21.19 ± 0.033	26.09 ± 1.305	8.93 ± 0.446
BSA	12.19 ± 0.545	14.38 ± 0.719	4.85 ± 0.243
CaM	10.90 ± 0.610	13.40 ± 0.700	2.15 ± 0.108

In the above investigations, gold nanoparticles preparation was as follows. N-Hydroxysuccinimide Ester (NHS)-activated 100 nm gold nanoparticles (Cytodiagnosics, Ontario, Canada) were conjugated via primary amine chemistry to the surface lysines of BSA (Sigma), lysozyme (Sigma Aldrich, St. Louis, Mo.) or calmodulin (Enzo Life Sciences, Farmingdale, N.Y.) following standard protocols. Briefly, proteins were diluted in 20 mM Hepes pH 7.4 containing 100 mM NaCl. Each conjugation reaction was initiated with addition of the proteins at a final volume of 0.133 mg/mL and gently agitated at room temperature for 2 hours. 10 μL of 1.0 M Tris was added to 990 μL of the particle solution to block any NHS groups remaining on the beads' surfaces. Samples were incubated with 1.0 M Tris with agitation for another hour then centrifuged for 30 minutes at 400×g to remove liquid. Conjugated samples were resuspended in NaCl-free buffer, to minimize any size variation due to charge effects, and their size and Pdl were measured using a Zetasizer (Malvern, United Kingdom). A schematic of the conjugation method is described in FIG. 4.

Polystyrene particle preparation was as follows. 300 nm, 520 nm, 1 μm, and 2 μm red fluorescent polystyrene particles (Fluoro-Max, Thermo Scientific, MA, USA) were centrifuged according to the manufacturer's protocols and resuspended in 20 mM Hepes pH 7.4 in order to maintain similar buffer settings to the prepared gold nanoparticles. The particles were ultrasonicated for 15 seconds in order to ensure full dispersion and resuspension. Particle size was measured using a Zetasizer (Malvern, United Kingdom).

Zeta potential was measured using both Malvern Zetasizer's Nano ZS and Nano ZS90 models. Measurements were taken to ensure that both instruments provided the same readings. All samples were analyzed using Dynamic Light Scattering (DLS) to determine their hydrodynamic radius and the polydispersity of the sample (Pdl). Standard 1 mL disposable polystyrene cuvettes were used (DTS0012, Malvern Instruments, Westborough, Mass.). Additionally the Zeta potentials of these modifications were recorded with DTS1060 cuvettes (Malvern Instruments, Westborough, Mass.).

Transmission electron microscopy (TEM) was performed using 400 mesh Formvar carbon coated copper grids (Electron Microscopy Sciences, FCF400-Cu-50) for imaging. First, the grids were treated with glow discharge in order to facilitate wetting of the surface. 5 μL of the gold particle sample was placed onto the mesh for 2 minutes followed by negative staining with 0.2% uranyl acetate (UA) in order to discern the protein layer on the particle surface. Samples were imaged with a Tecnai T20 TEM (FEI, Hillsboro, Oreg.) and processed using Gatan Digital Micrograph.

PD was performed as follows. Glass cover slips (No. 1 Thickness, Erie Scientific, Portsmouth, N.H.) were rinsed and sonicated with water, acetone, isopropanol, and ethanol sequentially and dried with compressed air. The surfaces were treated using corona discharge for wettability of the sample. 2 millimeter thick adhesive silicon wells (HT315, McMaster-Carr, Elmhurst, Ill.) were adhered onto the glass

cover slips. Seven microliters of nanoparticle samples were pipetted into the fluid chambers and covered with a second glass cover slip. The liquid touched both the top and bottom surface to form complete liquid bridge in order to avoid free surfaces which otherwise induced both vibrations as well as evaporative effects of the solution. The 100 nm gold nanoparticle samples were observed using dark field microscopy due to Rayleigh scattering. Dark field microscopy was performed using a 0.9 NA dark field air condenser (Nikon) and adapted onto an inverted microscope (Nikon Eclipse TE2000-U). 300 nm, 520 nm, 1 μm, and 2 μm particles were imaged using fluorescence microscopy via a fluorescent illumination lamp (Xcite series 120PC, EXFO Life Sciences & Industrial Division, Canada) attached to the inverted microscope. The objective used was 40×ELWD with a numerical aperture of 0.6. The movements of these diffraction-limited spots are imaged using a CCD camera with 1200×1600 pixel resolution with 2×2 binning at 13.3 fps (16-bit grayscale PCO.1600, PCO AG, Germany). Individual pixel size was 7.4×7.4 μm². Image acquisition was controlled using PCO software (CamWare V3.07, PCO AG, Germany). In order to maintain the same temperature and viscosity conditions for assuming ratiometric diffusion coefficients, PD measurements of all prepared particle samples were taken within hours of each other. Using our camera setup we have 3000 to 4000 particles in the microscope's field-of-view. 100 frames were recorded per PD measurement. 100 images were used in order to discern the change of Brownian motion between the different particle solutions while maintaining short time durations for potential comparison between this technique and other laboratory sizing equipment. For the Pdl measurements with PD, measurements were performed in triplicate in order to compare with DLS, which also performs its measurements in groups of three.

Dark field images resulting from the PD were analyzed in EDPIV, a PIV analysis software. The interrogation window (area) was determined as the average display in which 8 to 10 particles were maintained within the window. Data was either ensemble averaged (for ratiometric diffusion coefficient) or individually measured per interrogation window (for Pdl). Correlation data was post-processed and fit to a 5-point Gaussian distribution. The correlation peak width were calculated for both cross-correlation (sc) and autocorrelation (sa) data to determine the diffusion coefficient using an in-house MATLAB code.

In view of the above investigations, the PD process described herein uses dark field or fluorescence imagery for diffusometry of a non-flowing fluid sample having a relatively small volume, providing for characterization of particles much smaller than previously possible. In addition, PD may use diffusometry to determine the polydispersity index of the particles. If desired, PD provides the ability to predict the number of protein layers on the particles based on the polydispersity index and Brownian motion of the particles.

While the invention has been described in terms of specific or particular embodiments and investigations, it is apparent that other forms could be adopted by one skilled in the art. For example, the analyzer and its components could differ in appearance and construction from the embodiments described herein and shown in the drawings, functions of certain components of the analyzer could be performed by components of different construction but capable of a similar (though not necessarily equivalent) function, processing parameters such as temperatures and durations could be modified, and steps of PD could be performed using other devices. Accordingly, it should be understood that the inven-

15

tion is not limited to any embodiment described herein or illustrated in the drawings. It should also be understood that the phraseology and terminology employed above are for the purpose of describing the disclosed embodiments and investigations, and do not necessarily serve as limitations to the scope of the invention. Therefore, the scope of the invention is to be limited only by the following claims.

The invention claimed is:

1. A system comprising:

an imaging device;

means for recording a series of images of a fluid sample comprising particles suspended therein over a period of time;

means for analyzing the series of images to determine an average displacement of the particles over the time period using a cross-correlation that correlates an area from a first image of the series of images obtained at a first time (t_1) with the area from a second image of the series of images subsequently obtained at a second time (t_2); and

means for determining a diffusion coefficient of the particles based on the average displacement of the particles using the cross-correlation;

wherein the particles have biomolecules bound thereto, and the system further comprises means for determining an average thickness of the biomolecules bound to the particles based on the diffusion coefficient.

2. The system of claim 1, further comprising means for determining the uniformity of the particles within the fluid sample based on the diffusion coefficient.

3. The system of claim 1, further comprising means for determining a number of biomolecule layers on the particles and a variation of the number of biomolecule layers on the particles.

4. The system of claim 1, wherein the system is configured to analyze particles having a diameter or maximum dimension of two micrometers or less.

5. The system of claim 1, wherein the analyzing means further uses a second correlation and the determining means calculates the diffusion coefficient from peak widths of the cross-correlation and the second correlation.

6. The system of claim 5, wherein the determining means calculates the diffusion coefficient from the peak widths of the cross-correlation and the second correlation using:

$$D = \frac{s_c^2 - s_a^2}{16M^2\Delta t}$$

where D is the diffusion coefficient, s_c and s_a are, respectively, the peak widths of the cross-correlation and the second correlation measured at 1/e of peak heights thereof, M is magnification under which the series of images were recorded, and Δt is time between the first and second times (t_1, t_2).

7. A method comprising:

providing a sample having particles suspended in a fluid; obtaining and recording at least first and second images of the sample, the first image obtained at a first time (t_1) and the second image subsequently obtained at a second time (t_2);

determining an average displacement of the particles in an area of the first and second images during a time period (Δt) between the first time (t_1) and the second time (t_2) using a cross-correlation that correlates the area from the first and second images; and then

16

determining a diffusion coefficient of the particles in the area of the first and second images based on the average displacement of the particles during the time period (Δt) using the cross-correlation;

wherein the particles have biomolecules bound thereto, further comprising characterizing the conjugation of the biomolecules and the particles, wherein an increase in an absolute hydrodynamic radius of the particles relates to a decrease in the diffusion coefficient of the particles.

8. The method of claim 7, further comprising determining the uniformity of the particles within the sample based on the diffusion coefficient.

9. The system of claim 7, further comprising determining an average thickness of the biomolecules bound to the particles based on the diffusion coefficient.

10. The system of claim 7, further comprising determining a number of biomolecule layers on the particles and a variation of the number of biomolecule layers on the particles.

11. The method of claim 7, wherein the determining of the average displacement of the particles further uses a second correlation and the determining of the diffusion coefficient of the particles calculates the diffusion coefficient from peak widths of the cross-correlation and the second correlation.

12. The method of claim 11, wherein the determining of the diffusion coefficient of the particles calculates the diffusion coefficient from peak widths of the cross-correlation and the second correlation using:

$$D = \frac{s_c^2 - s_a^2}{16M^2\Delta t}$$

where D is the diffusion coefficient, s_c and s_a are, respectively, the peak widths of the cross-correlation and the second correlation measured at 1/e of peak heights thereof, M is magnification under which the series of images were recorded, and Δt is the time period between the first and second times (t_1, t_2).

13. A method comprising:

providing a sample having particles suspended in a fluid; obtaining and recording a series of images of the sample over a period of time;

partitioning each of the series of images into interrogation areas;

determining the average displacement of the particles in each of the interrogation areas in each of the series of images over the time period;

determining a diffusion coefficient of the particles in each of the interrogation areas in each of the series of images based on the average displacement of the particles; and then

determining an average diffusion coefficient of the particles by averaging the diffusion coefficients in each of the interrogation areas in each of the series of images.

14. The method of claim 13, wherein the particles have biomolecules bound thereto, wherein the diffusion coefficient of the particles is represented in the determining step as a ratio of particles without biomolecules bound thereto to biomolecule conjugated particles.

15. The method of claim 13, wherein the particles have biomolecules bound thereto, further comprising characterizing the conjugation of the biomolecules and the particles,

wherein an increase in an absolute hydrodynamic radius of the particles relates to a decrease in the diffusion coefficient of the of the particles.

16. The method of claim 13, further comprising determining a number of biomolecule layers on the particles and a variation of the number of biomolecule layers on the particles. 5

17. The method of claim 13, wherein the determining of the average displacement of the particles uses an autocorrelation and uses a cross-correlation that correlates in each of the interrogation areas in each of the series of images over the time period, and the determining of the diffusion coefficients of the particles calculates the diffusion coefficients from peak widths of the autocorrelation and the cross-correlation. 15

* * * * *



US 20180195944A1

(19) **United States**

(12) **Patent Application Publication**

Wereley et al.

(10) **Pub. No.: US 2018/0195944 A1**

(43) **Pub. Date: Jul. 12, 2018**

(54) **METHODS OF MEASURING STRUCTURAL AND FUNCTIONAL CHANGES OF A BIOMOLECULAR COMPOSITION**

Related U.S. Application Data

(60) Provisional application No. 62/436,081, filed on Dec. 19, 2016.

(71) Applicant: **Purdue Research Foundation**, West Lafayette, IN (US)

Publication Classification

(72) Inventors: **Steven Truitt Wereley**, West Lafayette, IN (US); **Tamara Lea Kinzer-Ursem**, West Lafayette, IN (US); **Katherine Noel Clayton**, West Lafayette, IN (US); **Jacqueline Callihan Linnes**, West Lafayette, IN (US); **Donghoon Lee**, West Lafayette, IN (US); **Taylor Jo Moehling**, West Lafayette, IN (US)

(51) **Int. Cl.**
G01N 11/10 (2006.01)
G01N 15/14 (2006.01)

(52) **U.S. Cl.**
CPC *G01N 11/10* (2013.01); *G01N 2015/0053* (2013.01); *G01N 15/1429* (2013.01)

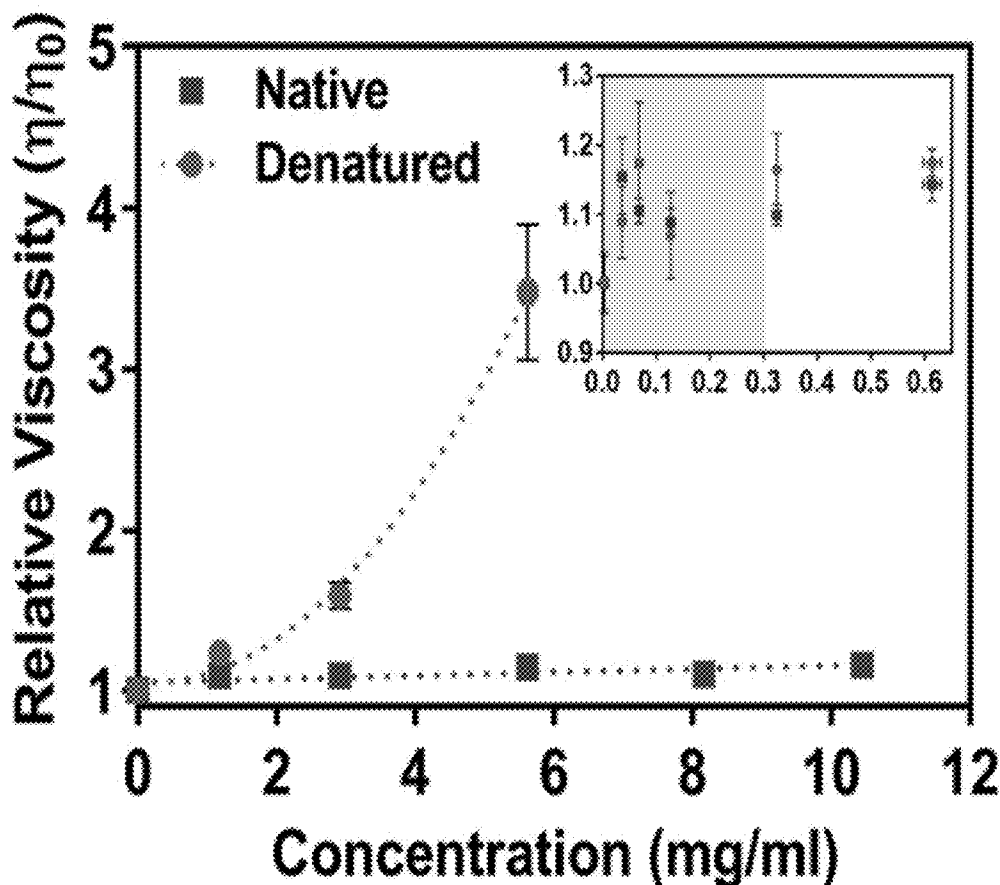
(73) Assignee: **Purdue Research Foundation**, West Lafayette, IN (US)

(57) **ABSTRACT**

This invention relates to a method for measuring viscosity of a fluid using particle diffusometry (PD). The method finds practical applications in detecting structural and functional changes of a biomolecular composition by comparing the viscosity change as compared with the standard of the biomolecular composition. This method may also find uses in clinical diagnosis and quality control of clinical biological medicines, food and feeds during the process of manufacturing, distribution and consumption.

(21) Appl. No.: **15/846,430**

(22) Filed: **Dec. 19, 2017**



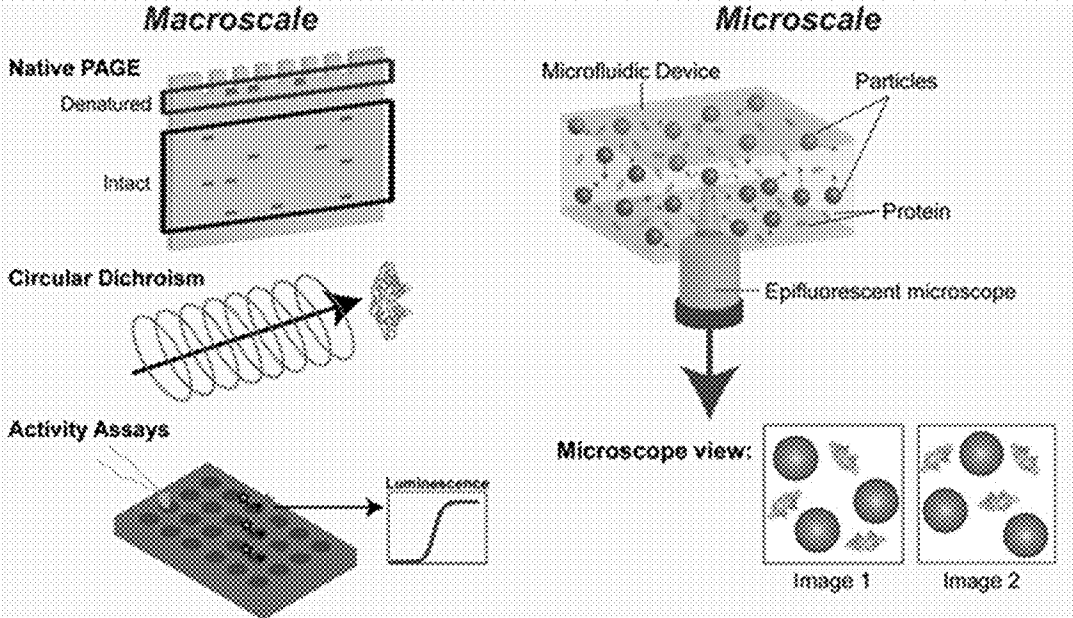


FIG. 1

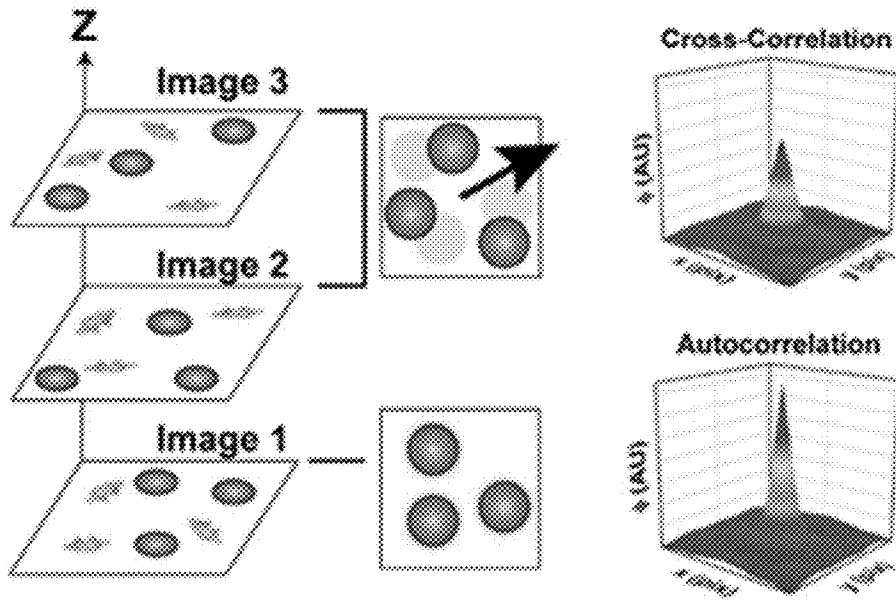


FIG. 2

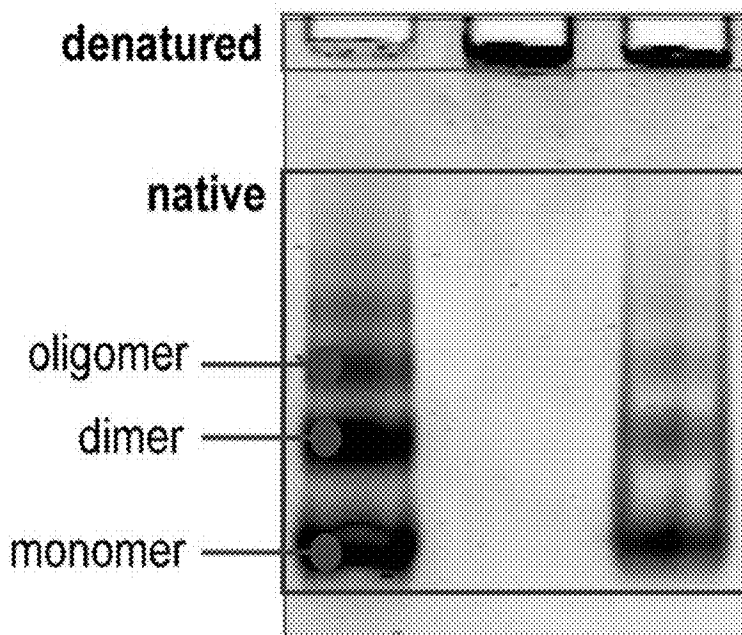


FIG. 3A

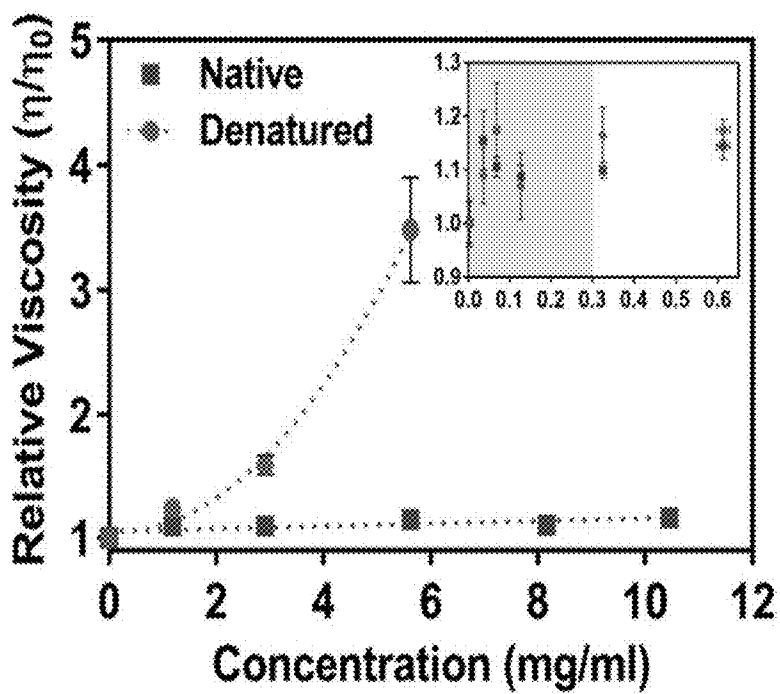


FIG. 3B

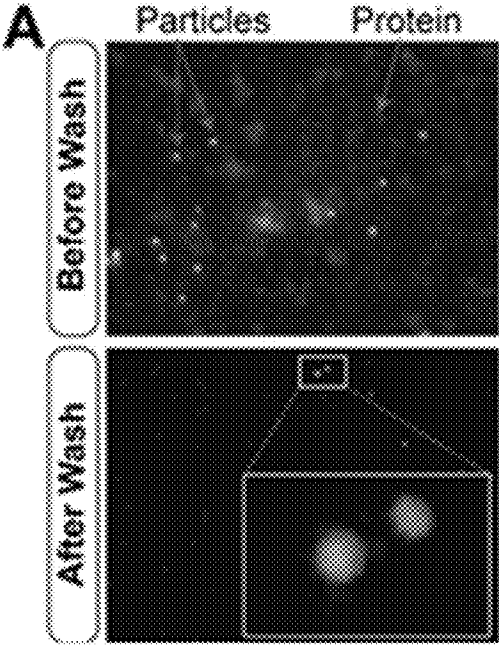


FIG. 4A

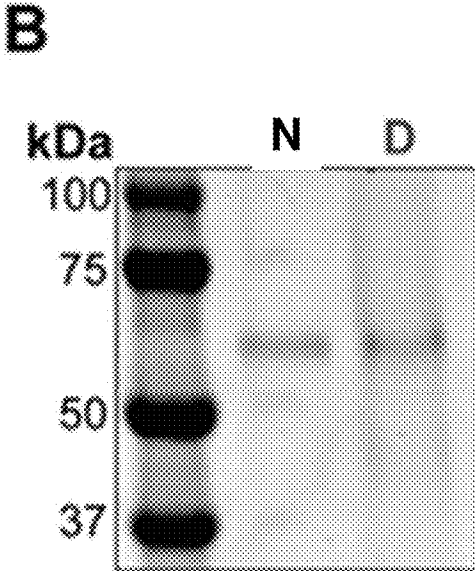


FIG. 4B

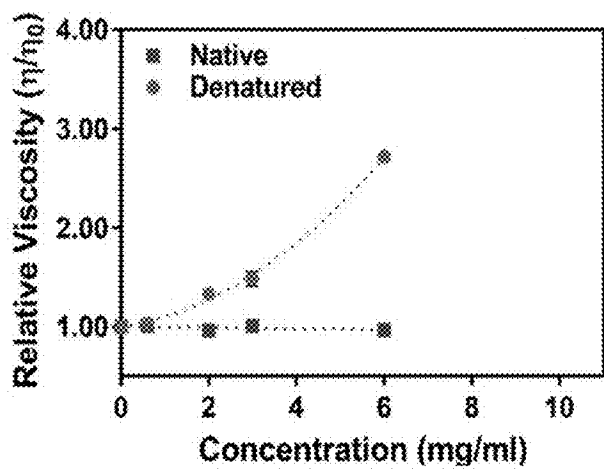


FIG. 5A

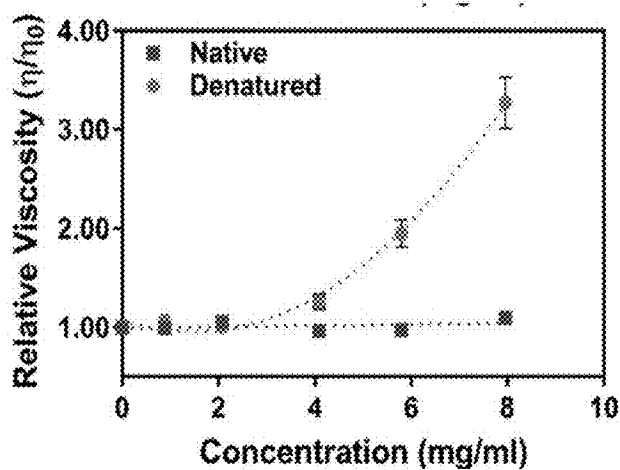


FIG. 5B

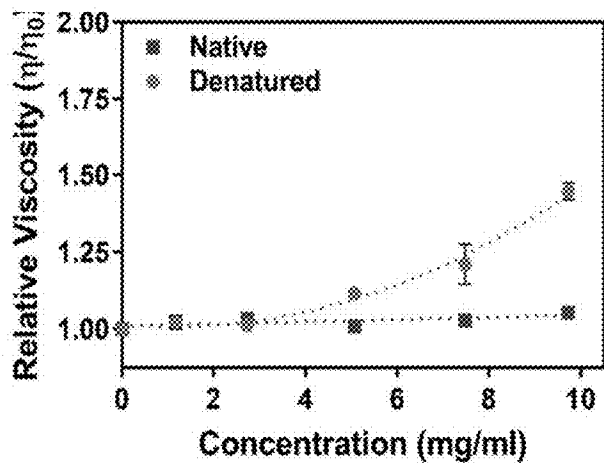


FIG. 5C

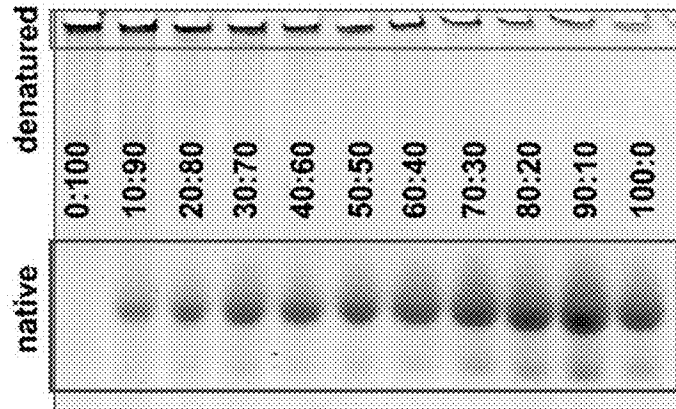


FIG. 6A

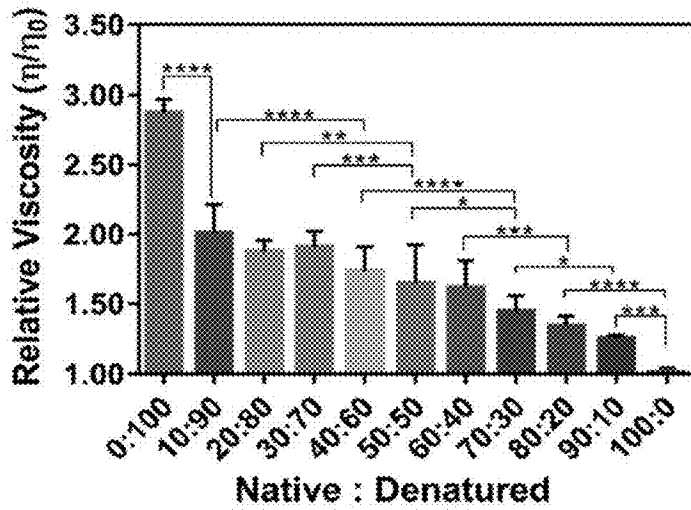


FIG. 6B

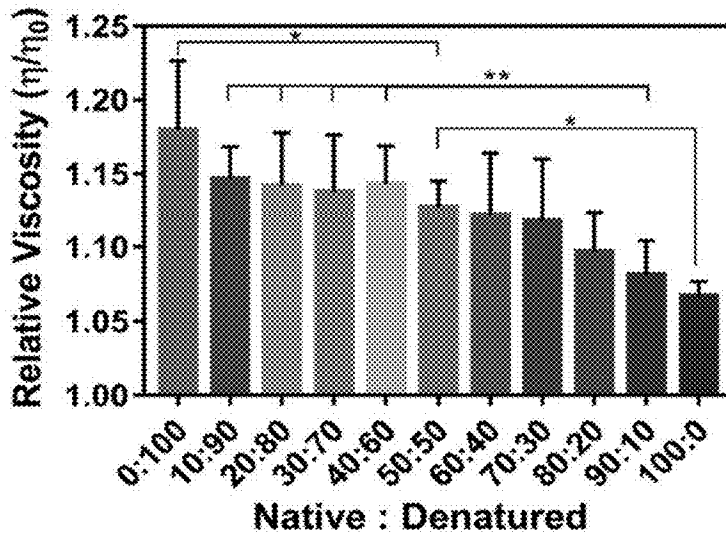


FIG. 6C

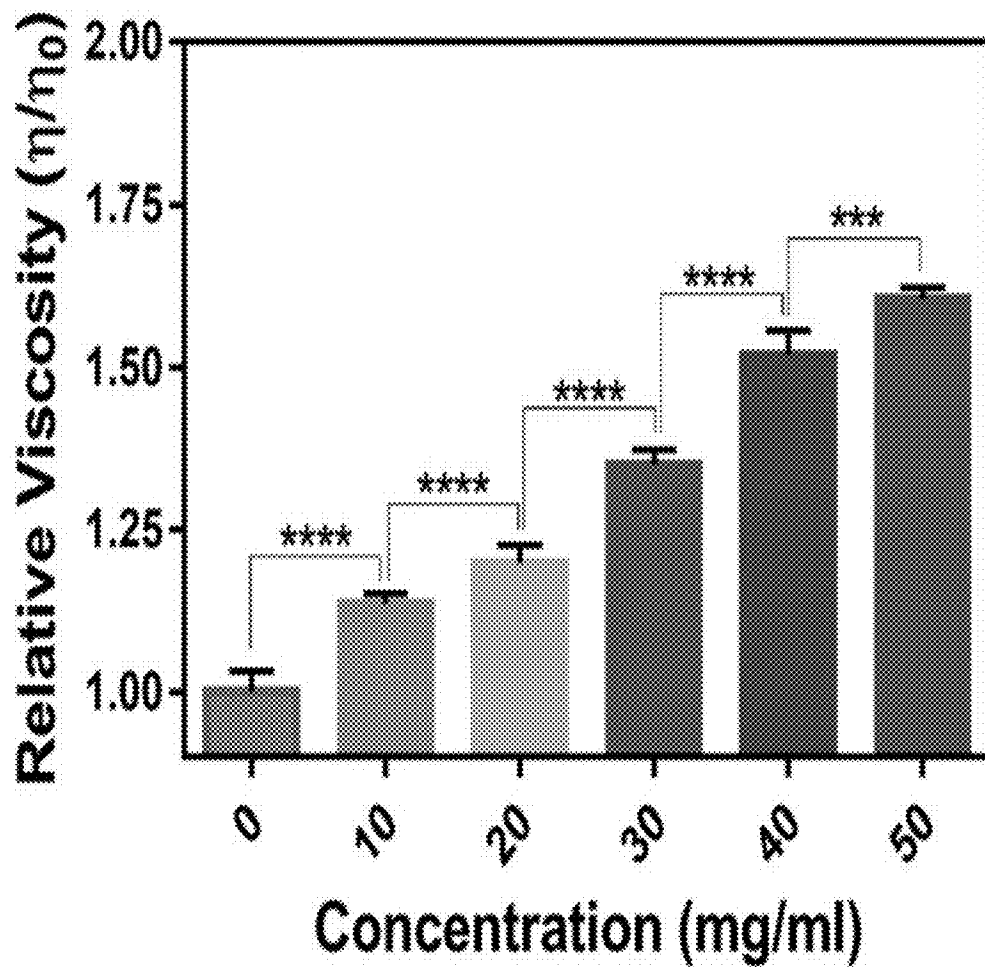


FIG. 7

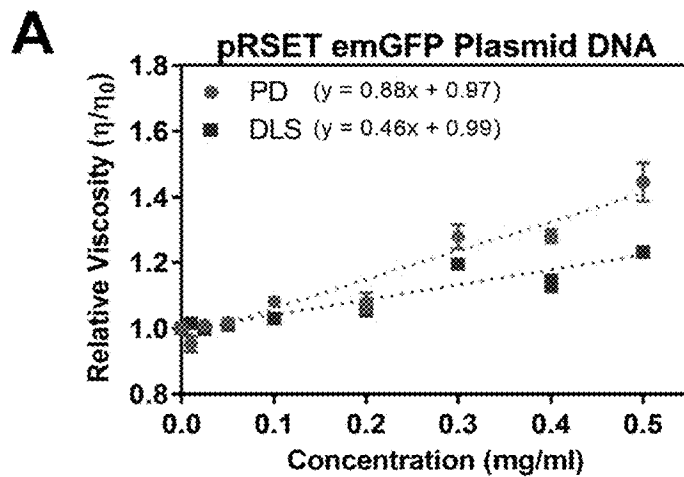


FIG 8A

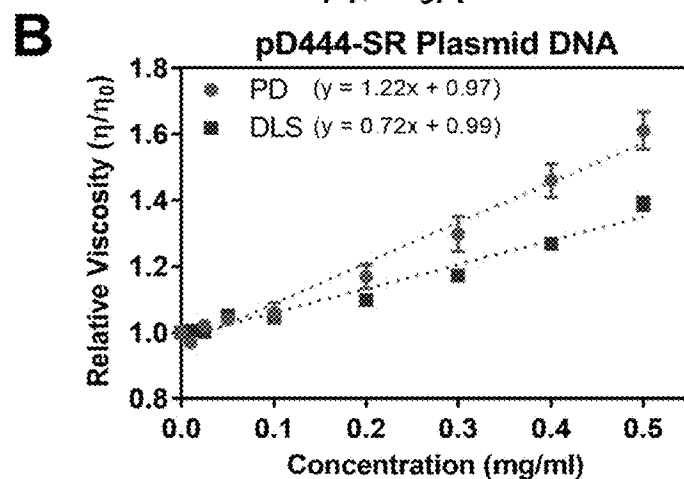


FIG 8B

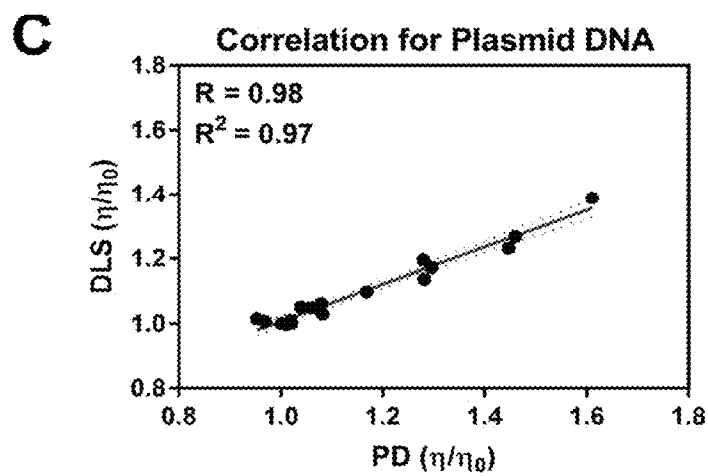


FIG. 8C

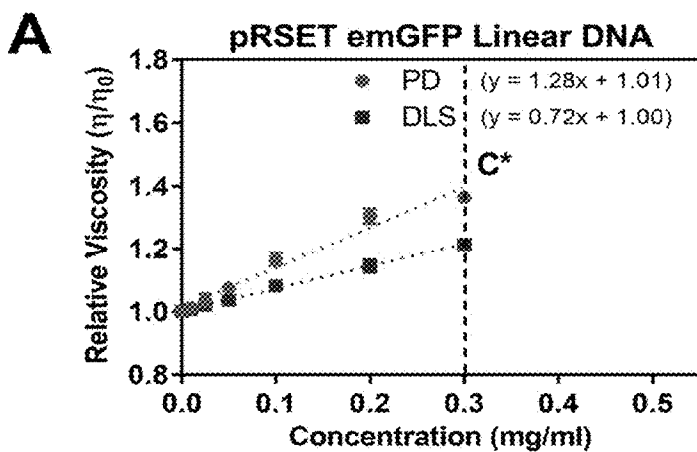


FIG 9A

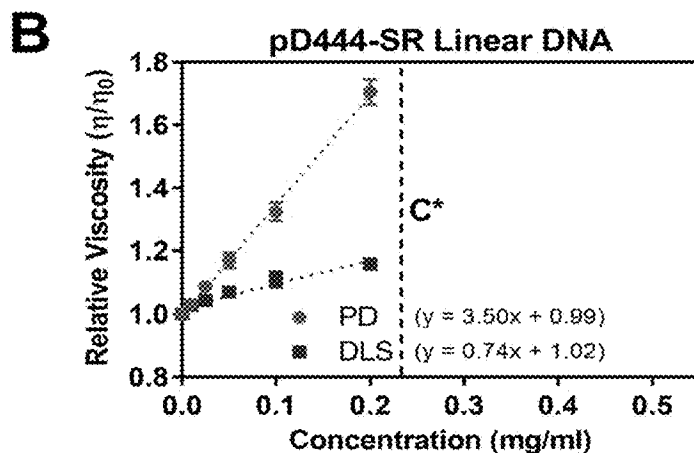


FIG. 9B

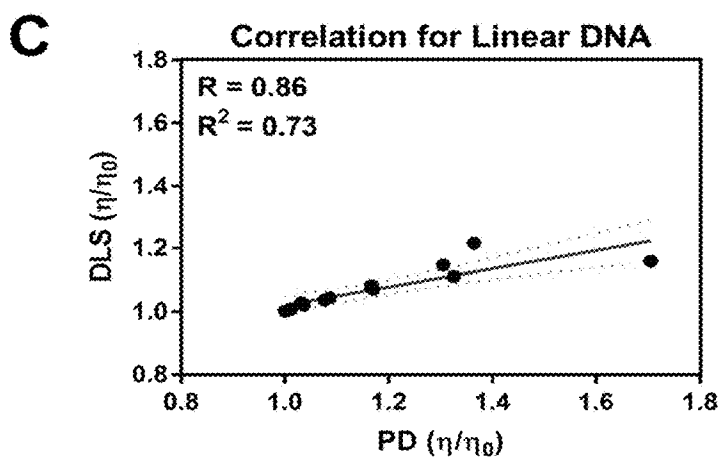


FIG. 9C

METHODS OF MEASURING STRUCTURAL AND FUNCTIONAL CHANGES OF A BIOMOLECULAR COMPOSITION

CROSS-REFERENCE TO RELATED APPLICATIONS

[0001] The present U.S. patent application is related to and claims the priority benefit of U.S. Provisional Patent Application Ser. No. 62/436,081, filed Dec. 19, 2016, the contents of which are hereby incorporated by reference in their entirety into this disclosure.

TECHNICAL FIELD

[0002] This invention relates to a method for measuring viscosity of a fluid using particle diffusometry (PD). The method finds practical applications in detecting structural and functional changes of a biomolecular composition by comparing the viscosity change as compared with the standard of the biomolecular composition. This method may also find uses in clinical diagnosis and quality control of clinical biological medicines, food and feeds during the process of manufacturing, distribution and consumption.

BACKGROUND

[0003] This section introduces aspects that may help facilitate a better understanding of the disclosure. Accordingly, these statements are to be read in this light and are not to be understood as admissions about what is or is not prior art.

[0004] Peptide- and protein-based biological therapeutics, as compared with the traditional, orally dosed small molecule drugs, are not orally bioavailable. Those biological medical products are normally formulated as an injectable solution. Due to the inherent structural instability of those proteins and peptides, it is imperative to monitor any structural changes of those compounds during storage and transportation, and before the targeted human use. For example, human insulin is a peptide of 51 amino acid residues, which is commonly formulated as an injectable solution and widely used to treat both type I and type II diabetes.

[0005] Over 400 million people worldwide suffer from diabetes (Rubino, et al, *Nature* 2016, 533, 459-461). For diabetes type I and many type II patients, insulin is a biopharmaceutical widely used to maintain consistent glucose levels within the blood. Therefore, maintaining native protein folding of insulin is essential for biopharmaceutical function. In turn, the global insulin market size is expected to reach \$53.04 billion by 2020. Although there is a large population affected by diabetes and therefore a growing global insulin market, there is currently no method at the point of care in which patients can determine if their insulin is still effective. Monitoring insulin efficacy is critical considering that the state of the biopharmaceutical diminishes due to both temperature and time. Present measures to determine the effectiveness of insulin include (1) patients returning their prescription to the manufacturer for examination, (2) trial injection of the drug and examining the outcome, or (3) simply purchasing a new prescription. These current approaches are either unsafe, inadequate, or come at monetary cost.

[0006] Designing miniaturized platforms for analyzing biopharmaceutical degradation provides significant advantages to current macroscale systems. These include the

ability to investigate the quality of the pharmaceutical at both the sites of clinical care and patient homes while using minimal sample volumes. Current screening processes of protein-based biopharmaceuticals are inaccessible to the public since drug screening is performed in-house. Therefore, patients have no method for tracking the safety and efficacy of their pharmaceutical prescriptions—which often occurs due to incorrect storage conditions or age of the product. Since there is no existing method to study biopharmaceutical expiration at the point of care, this opens up a new research realm to develop a method to screen for the degradation of protein-based biopharmaceuticals. The present disclosure provides a practical solution to those unmet needs.

SUMMARY

[0007] This invention relates to a method for measuring viscosity of a fluid using particle diffusometry (PD). The method finds practical applications in detecting structural and functional changes of a biomolecular composition by comparing the viscosity change as compared with the standard of the biomolecular composition. This method may also find uses in clinical diagnosis and quality control of clinical biological medicines, food and feeds during the process of manufacturing, distribution and consumption.

[0008] In some illustrative embodiments, the present invention discloses a method for measuring viscosity of a liquid comprising the steps of:

[0009] a. preparing a testing solution using said liquid with added uniformly sized particles of about 50–1,000 nm.

[0010] b. capturing a plurality of microscopic images of said particles in said testing solution over a period of time;

[0011] c. partitioning each of the plurality of images into interrogation regions and determining the average displacement of the particles in each of the interrogation regions of the plurality of images over said time period;

[0012] d. determining diffusion coefficient of the particles based on the average displacement of the particles; and

[0013] e. calculating viscosity of said liquid using determined diffusion coefficient with Einstein's diffusion equation.

[0014] In some other illustrative embodiments, the present invention discloses a method for measuring viscosity of a liquid, wherein the uniformly sized particles are made of gold, silver, polystyrene, or similar structurally stable materials. In some instance, the particles are fluoresce or isotopic labeled or magnetic.

[0015] In some other illustrative embodiments, the present invention discloses a method for measuring viscosity of a liquid, wherein the liquid is a biomolecular composition selected from the group consisting of nucleic acid, amino acid, lipid, peptide, protein, antibody, enzyme, carbohydrate, DNA, RNA, polysaccharide, oligonucleotide, oligosaccharide, proteoglycans, and glycoprotein.

[0016] In some other illustrative embodiments, the present invention discloses a method for measuring viscosity of a liquid, wherein said biomolecular composition is a biological therapeutics.

[0017] In some other illustrative embodiments, the present invention discloses a method for measuring viscosity of a

liquid, wherein the method is used for measuring structural and functional changes of a biomolecular composition of testing subject from a standard thereof, comprising the steps of:

- [0018] a. measuring viscosity of the biomolecular composition of testing subject;
 - [0019] b. measuring viscosity of the standard biomolecular composition of testing subject; and
 - [0020] c. comparing viscosity of said biomolecular composition of testing subject with that of said standard, wherein finding of a substantial difference suggests structural and functional changes of said biomolecular composition of testing subject.
- [0021] In some other illustrative embodiments, the present invention discloses a method for measuring structural and functional changes of a biomolecular composition of testing subject from a standard thereof, comprising the steps of:
- [0022] a. preparing a testing solution using said biomolecular composition with added uniformly sized particles of about 50–1,000 nm.
 - [0023] b. capturing a plurality of microscopic images of said particles of said testing solution over a period of time;
 - [0024] c. partitioning each of the plurality of images into interrogation regions and determining the average displacement of the particles in each of the interrogation regions of the plurality of images over said time period;
 - [0025] d. determining a diffusion coefficient based on the average displacement of the particles;
 - [0026] e. calculating viscosity of said biomolecular composition of testing subject using the determined diffusion coefficient with Einstein's diffusion equation;
 - [0027] f. obtaining viscosity of a standard biomolecular composition of testing subject by repeating steps a.–e.; and
 - [0028] g. comparing viscosity of said biomolecular composition of testing subject and that of said standard thereof, wherein finding of a substantial difference suggests structural and functional changes of said biomolecular composition.
- [0029] In some illustrative embodiments, the present invention discloses a method for measuring structural and functional changes of a biomolecular composition, wherein said biomolecular composition comprises one or more of biomolecules selected from the group consisting of amino acid, lipid, peptide, protein, antibody, enzyme, carbohydrate, DNA, RNA, polysaccharide, oligonucleotide, oligosaccharide, proteoglycans, and glycoprotein.

BRIEF DESCRIPTION OF THE DRAWINGS

[0030] Embodiments of the present disclosure will now be described by way of example in greater detail with reference to the attached figures, in which:

- [0031] FIG. 1 describes the gold standard macroscale systems for measuring protein folding state involve methods such as native PAGE, circular dichroism, and activity assays. Conversely, particle diffusometry (PD), a microscale system, involves imaging particles suspended in a protein solution and correlating the motion to determine sample viscosity, and therefore protein folding state;
- [0032] FIG. 2 shows a stack of images that are correlated with themselves produce an autocorrelation peak (Image 1). The correlation of sequential images (Image 2 with Image 3)

provides the cross-correlation peaks. Note that the cross-correlation peak is both wider and shorter as compared to the autocorrelation peak;

[0033] FIG. 3A is a native polyacrylamide gel electrophoresis (PAGE) of native and denatured BSA at a concentration of 0.25 mg/mL. The denatured BSA remains at the channel entrance of the gel (top, red box) and native samples propagate into the gel (bottom, blue box). The left lane contains only native BSA, the middle lane contains only heat treated, denatured BSA, and the third, rightmost lane contains a mixture of 50% native and 50% degraded BSA;

[0034] FIG. 3B shows the PD measurement of the viscosity of BSA solutions relative to the buffer solution. The relative viscosity of denatured BSA solutions (red circles) increases as the concentration of the protein increases, whereas the viscosity of solutions containing native protein (blue squares) remains constant as a function of concentration. The viscous effects from lower protein concentrations are statistically indistinguishable from one another as both a function of concentration and protein folding state (inset, highlighted in the peach region); n=9;

[0035] FIG. 4A shows analysis of nonspecific protein adsorption on particle surfaces. Prior to washing, particles in the presence of 5 mg/mL FITC labeled BSA show green fluorescent background signal, indicating free protein (top). After washing (bottom) the background fluorescent signal is dramatically reduced as expected, with concentrated fluorescent green signal located around the red particle circumference indicating non-specific adsorption of FITC-BSA to the particles;

[0036] FIG. 4B presents the SDS-PAGE analysis of the 5 mg mL⁻¹ BSA sample non-specifically absorbed to beads for both native (N) and denatured (D) BSA samples indicate similar levels of non-specific adsorption;

[0037] FIG. 5A shows the relative viscosity of denatured insulin increases as the concentration of the protein increases in PBS (1x) at pH 2.5, where there is a dramatic difference in the viscosity of denatured insulin at 2 mg/mL;

[0038] FIG. 5B shows native insulin solubilized in HEPES at pH 2.5, where there is a statistically significant difference in viscosity at a concentration of 4 mg/mL;

[0039] FIG. 5C shows insulin samples in HEPES at pH 8.2 where there is the least dramatic difference in viscosity of insulin, but nonetheless there is a non-linear increase in solution viscosity for denatured protein sample; n=9;

[0040] FIG. 6A shows a native PAGE of different mixtures of native and denatured insulin, where more denatured insulin produces a higher viscosity;

[0041] FIG. 6B shows the relative viscosity of different mixtures of native and denatured insulin in PBS at pH 2.5 (v/v ratio);

[0042] FIG. 6C shows the relative viscosity of different mixtures of native and denatured insulin in HEPES at pH 8.2 (v/v ratio). As the ratio of denatured insulin increases, the relative viscosity also increases. Note the relative viscosity on the y-axis is different between FIG. 6B and FIG. 6C (* indicates p<0.05, ** p<0.01, *** p<0.001, **** p<0.0001, n=9); and

[0043] FIG. 7 shows the relative viscosity of an antibody. As the concentration of IgG antibody solution increases, the relative viscosity of the solution increases (****p<0.0001, *** p<0.001, n=9; measurements are relative to the buffer in which IgG is suspended in).

[0044] FIG. 8A shows relative solution viscosity was measured with PD and DLS as a function of increasing 3618 bp pRSET emGFP plasmid concentration.

[0045] FIG. 8B shows Changes in solution viscosity as a function of circular plasmid DNA concentration by increasing 6162 bp pD444-SR plasmid concentration. Measurements were relative to QIAGEN elution buffer. n=3 independent experiments.

[0046] FIG. 8C demonstrates that DLS and PD measurements were highly positively correlated. Pearson Correlation Coefficient=0.98.

[0047] FIG. 9A shows relative solution viscosity as measured with PD and DLS as a function of increasing 3618 bp pRSET emGFP linear plasmid concentration.

[0048] FIG. 9B describes Changes in solution viscosity as a function of linear plasmid DNA concentration by increasing 6162 bp pD444-SR linear plasmid concentration. DNA concentrations below the critical concentration are marked by a dotted line. Measurements are relative to QIAGEN elution buffer. n=3 independent experiments.

[0049] FIG. 9C demonstrates that DLS and PD measurements were highly positively correlated. Pearson Correlation Coefficient=0.85. The dashed lines indicate a 95% confidence interval.

DETAILED DESCRIPTION

[0050] For the purposes of promoting an understanding of the principles of the present disclosure, reference will now be made to the embodiments illustrated in the drawings, and specific language will be used to describe the same. It will nevertheless be understood that no limitation of the scope of this disclosure is thereby intended.

[0051] In the present disclosure the term “about” can allow for a degree of variability in a value or range, for example, within 20%, within 10%, within 5%, or within 1% of a stated value or of a stated limit of a range.

[0052] In the present disclosure the term “substantially” can allow for a degree of variability in a value or range, for example, within 80%, within 90%, within 95%, or within 99% of a stated value or of a stated limit of a range.

[0053] Terminology surrounding biopharmaceuticals varies between groups and entities, with different terms referring to different subsets of therapeutics within the general biopharmaceutical category. Some regulatory agencies use the terms biological medicinal products or therapeutic biological product to refer specifically to engineered macromolecular products like protein- and nucleic acid-based drugs, distinguishing them from products like blood, blood components, or vaccines, which are usually extracted directly from a biological source (Ronald A Rader, *Nature Biotechnology* 26, 743-751 (2008)). In practice, biologics includes a wide range of products such as vaccines, blood and blood components, allergenics, somatic cells, gene therapy, antibody, therapeutic oligonucleotides, tissues and recombinant therapeutic proteins. Most biopharmaceuticals are classed and regulated by FDA as biologics. However, due to their similarity to products historically regulated as drugs, some simpler biopharmaceuticals are regulated as drugs, mostly recombinant hormones, for example, insulin and human growth hormone. Some overlapping exists between biopharmaceuticals and drugs. Biological medicine, biological therapeutics, and biomolecular therapeutics are used interchangeably.

[0054] As disclosed herein, the particles used in the Particle Diffusometry (PD) are beads or microbeads that we add to the testing system. Those beads can be made of any structurally stable materials. For example, uniformly sized beads of polystyrene or gold particles are commonly used in the development of the ideas disclosed in this invention. In some instances, those beads are fluorescently labeled or dyed. In some instances, the choice of the particles depends on the sensitivity needed and the imaging system employed. For example, we use 100 nm gold particles for dark field imaging, or fluorescent polystyrene particles around 200 nm for diagnostic purpose.

[0055] As disclosed herein, the captured images are transformed using Fast Fourier Transforms, then correlated using techniques that are standard digital image correlation techniques that are standard and well known in the field. MATLAB was used to carry out the transformations and digital image correlation.

[0056] This invention relates to a method for measuring viscosity of a fluid using particle diffusometry. The method finds practical applications in detecting structural and functional changes of a biomolecular composition by comparing the viscosity change as compared with the standard of the biomolecular composition. This method may also find uses in clinical diagnosis and quality control of clinical biological medicines, food and feeds during the process of manufacturing, distribution and consumption.

[0057] In some illustrative embodiments, the present invention discloses a method for measuring viscosity of a liquid comprising the steps of:

- [0058]** a. preparing a testing solution using said liquid with added uniformly sized particles of about 50–1,000 nm.
- [0059]** b. capturing a plurality of microscopic images of said particles in said testing solution over a period of time;
- [0060]** c. partitioning each of the plurality of images into interrogation regions and determining the average displacement of the particles in each of the interrogation regions of the plurality of images over said time period;
- [0061]** d. determining diffusion coefficient of the particles based on the average displacement of the particles; and
- [0062]** e. calculating viscosity of said liquid using determined diffusion coefficient with Einstein's diffusion equation.

[0063] In some other illustrative embodiments, the present invention discloses a method for measuring viscosity of a liquid, wherein the uniformly sized particles are made of gold, silver, polystyrene, or similar structurally stable materials. In some instance, the particles are fluoresce or isotopic labeled or magnetic.

[0064] In some other illustrative embodiments, the present invention discloses a method for measuring viscosity of a liquid, wherein the liquid is a biomolecular composition selected from the group consisting of nucleic acid, amino acid, lipid, peptide, protein, antibody, enzyme, carbohydrate, DNA, RNA, polysaccharide, oligonucleotide, oligosaccharide, proteoglycans, and glycoprotein.

[0065] In some other illustrative embodiments, the present invention discloses a method for measuring viscosity of a liquid, wherein said biomolecular composition is a biological therapeutics.

[0066] In some other illustrative embodiments, the present invention discloses a method for measuring viscosity of a liquid, wherein the method is used for measuring structural and functional changes of a biomolecular composition of testing subject from a standard thereof, comprising the steps of:

[0067] a. measuring viscosity of the biomolecular composition of testing subject;

[0068] b. measuring viscosity of the standard biomolecular composition of testing subject; and

[0069] c. comparing viscosity of said biomolecular composition of testing subject with that of said standard, wherein finding of a substantial difference suggests structural and functional changes of said biomolecular composition of testing subject.

[0070] In some other illustrative embodiments, the present invention discloses a method for measuring structural and functional changes of a biomolecular composition of testing subject from a standard thereof, comprising the steps of:

[0071] a. preparing a testing solution using said biomolecular composition with added uniformly sized particles of about 50–1,000 nm.

[0072] b. capturing a plurality of microscopic images of said particles of said testing solution over a period of time;

[0073] c. partitioning each of the plurality of images into interrogation regions and determining the average displacement of the particles in each of the interrogation regions of the plurality of images over said time period;

[0074] d. determining a diffusion coefficient based on the average displacement of the particles;

[0075] e. calculating viscosity of said biomolecular composition of testing subject using the determined diffusion coefficient with Einstein's diffusion equation;

[0076] f. obtaining viscosity of a standard biomolecular composition of testing subject by repeating steps a.–e.; and

[0077] g. comparing viscosity of said biomolecular composition of testing subject and that of said standard thereof, wherein finding of a substantial difference suggests structural and functional changes of said biomolecular composition.

[0078] In some illustrative embodiments, the present invention discloses a method for measuring structural and functional changes of a biomolecular composition, wherein said biomolecular composition comprises one or more of biomolecules selected from the group consisting of nucleic acid, amino acid, lipid, peptide, protein, antibody, enzyme, carbohydrate, DNA, RNA, polysaccharide, oligonucleotide, oligosaccharide, proteoglycans, and glycoprotein.

[0079] In one illustrative embodiment, the present invention is related to a method for measuring structural and functional changes of a biomolecular composition, wherein said biomolecular composition is prepared by combining individual components.

[0080] In one illustrative embodiment, the present invention is related to a method for measuring structural and functional changes of a biomolecular composition, wherein said biomolecular composition is derived from bodily fluids, cell cultures, environmental samples, air samples, water samples, soil samples, or other matrices that contain biomolecules.

[0081] In one illustrative embodiment, the present invention is related to a method for measuring structural and functional changes of a biomolecular composition, wherein said biomolecular composition is derived from a living organism including prokaryotic cells, eukaryotic cells, viruses, or prions.

[0082] In one illustrative embodiment, the present invention is related to a method for measuring structural and functional changes of a biomolecular composition, wherein said biomolecular composition is prepared by combining individual components.

[0083] In one illustrative embodiment, the present invention is related to a method for measuring structural and functional changes of a biomolecular composition, wherein the biomolecular composition is a therapeutics for treatment of a disease.

[0084] In one illustrative embodiment, the present invention is related to a method for measuring structural and functional changes of a biomolecular composition, wherein said biomolecular composition is a biotherapeutic formulation.

[0085] In one illustrative embodiment, the present invention is related to a method for measuring structural and functional changes of a biomolecular composition, wherein said biomolecular composition is an enzyme or an antibody formulation.

[0086] In one illustrative embodiment, the present invention is related to a method for measuring structural and functional changes of a biomolecular composition, wherein said biomolecular composition is a peptide, protein or glycoprotein formulation.

[0087] In some other illustrative embodiments, the present invention discloses a method for detecting presence of bacterial, viral, protozoa, fungal, or other parasitic contamination of a liquid, comprising the step of:

[0088] a. preparing a testing solution using said liquid with added uniformly sized particles of about 50–1,000 nm.

[0089] b. capturing a plurality of microscopic images of said micro particles of said testing solution over a period of time;

[0090] c. partitioning each of the plurality of images into interrogation regions and determining the average displacement of the particles in each of the interrogation regions of the plurality of images over said time period;

[0091] d. determining diffusion coefficient of the particles based on the average displacement of the particles;

[0092] e. calculating viscosity of said liquid using the determined diffusion coefficient with Einstein's diffusion equation;

[0093] f. obtaining viscosity of a non-contaminated standard of said liquid by repeating steps a.–e.; and

[0094] g. comparing viscosity of said liquid and that of said non-contaminated standard thereof, wherein finding of a substantial difference suggests presence of bacterial, viral, protozoa, fungal, or other parasitic contamination of said liquid.

[0095] In some illustrative embodiments, the present invention discloses a method for detecting presence of bacterial, viral, protozoa, fungal, or other parasitic contamination of a liquid, wherein said liquid is for human or animal consumption.

[0096] In some illustrative embodiments, the present invention discloses a method for detecting presence of bacterial, viral, protozoa, fungal, or other parasitic contamination of a liquid, wherein said liquid is selected from the group consisting of biological medicine, water, waste water of any source, fruit juice, vegetable juice, liquid food, and a liquid waste from a food or feed processing.

[0097] In some illustrative embodiments, the present invention discloses a method for detecting presence of bacterial, viral, protozoa, fungal, or other parasitic contamination of a liquid, wherein the method is used for quality control of biological medicines, food and feeds during the process of manufacturing, distribution and consumption.

[0098] In some illustrative embodiments, the present invention discloses a method for detecting presence of bacterial, viral, protozoa, fungal, or other parasitic contamination of a liquid, wherein the biological medicine is a biotherapeutic formulation.

[0099] In one illustrative embodiment, the present invention may be used in the quality control of a liquid formulation of the clinical medicines.

[0100] In another illustrative embodiment, the present invention may be used to monitor any bacterial and/or viral contamination of a liquid for human or animal consumption.

[0101] In one illustrative embodiment, the present invention may be configured as a portable device for quality control of a liquid formulation for human or animal consumption.

[0102] In one illustrative embodiment, the present invention may be configured as a portable device for point-of-care diagnosis of bacterial or viral infection.

[0103] Complex sample solutions with mixed conformations of biomolecules present a challenge for detection in point of care diagnostics. For example, insulin is widely used in diabetes care administered by patients themselves at home. Currently there is no method to monitor insulin at the point of care. Current gold-standard methods remain strictly in the laboratory space and at the macroscale which include techniques such as native polyacrylamide gel electrophoresis (PAGE), circular dichroism (CD), and protein activity assays. Native PAGE is a gel electrophoresis method which provides information on protein electrophoretic mobility, folding state, and sample purity. Native PAGE is widely implemented for a wide variety of protein-based studies. However, given that native PAGE is most often used by molecular biology and biochemistry researchers, it is clear that this technique is designed strictly for the laboratory space. Likewise, CD is a spectral technique involving a polarized light source to study protein conformation. This technique has been integral in furthering the investigation of protein structure and molecular interactions. Though similarly to native PAGE, CD it is not designed to be used by patients or clinicians, but rather structural biologists. Lastly, researchers are not only interesting in native protein morphology but also the activity of the protein itself. Methods used to assess protein activity involve precise reagent handling and luminescence readouts. Similarly to CD and native PAGE, activity assays are not feasible for patients to use due to the extensive training and analysis tools needed for assessment. Engineering a simple micro-scale device to study insulin degradation would provide patients with a monitoring device which could be used to track the efficacy of insulin.

[0104] Particle diffusometry (PD) has the capability to detect even minute differences in biomolecular compositions (Clayton, et al., *Biomicrofluidics* 2016, 10, 1-15). Based on the fundamental principles of diffusion, particles undergoing Brownian motion are imaged under fluorescence microscopy and particle motion is statistically quantified. Using particle diffusometry we rapidly quantify the presence of biomolecules by determining the change in the sample viscosity which is calculated through Einstein's diffusion equation. This passive viscosity measurement can be performed in micro-to-nanoliter volumes allowing particle diffusometry to be readily integrated into micro-total analysis systems.

[0105] This present invention disclosed a method to examine how intact and denatured proteins alter the viscosity of solutions using a novel particle diffusometry (PD). PD is statistically robust technique and therefore sensitive enough to experimentally determine minute changes in protein viscosity (Clayton, et al., 2016). Studying small changes in protein solutions is essential for biopharmaceutical research. By adding 200 nm fluorescent particles to a quiescent 4 μ L protein solution, we calculate the diffusion coefficient of these particles. PD correlates sequential images in order to statistically determine a diffusion coefficient using only 8 seconds of data. The diffusion coefficient allows us to calculate the viscosity of these protein samples using the Stokes-Einstein equation. PD is fundamentally different than particle tracking, a technique previously used for studying passive microrheology. Particle tracking calculates individual particle trajectories and averages them to determine a diffusion coefficient (Squires, et al., *Annu. Rev. Fluid Mech.* 2010, 42(1), 413-438; Mason, et al., *Phys. Rev. Lett.* 1997, 79(17), 3282-3285). Because this particle tracking approach requires averaging many particle trajectories to determine statistically relevant results, this takes time consuming and computationally intensive. Such an approach is not feasible in providing rapid results for biopharmaceutical analysis. Algorithms which provide rapid feedback are more likely to be integrated into devices for the patient's home or at a local clinic. Therefore, PD algorithms are practical to integrate with technologies directed toward the point of care.

[0106] Here we first investigate the protein bovine serum albumin (BSA) as a proof-of-principle. BSA is a well characterized protein often used in microfluidics. Using BSA we consider how the solution viscosity changes as a function of the protein's folding state and solution concentration. We believe that denatured BSA is more viscous than its intact counterpart. Additionally, we investigate how BSA concentration alters protein viscosity measurements. Based on the initial characterization of BSA we use this knowledge to study a pharmacologically relevant protein, insulin. We apply similar methods to study insulin that we performed with BSA. However, it should be noted that insulin is both structurally and electrostatically very different than our proof-of-principle BSA system. Finally, we realize that biopharmaceutical solutions are unlikely to be fully intact or degraded. This is due to transportation from the manufacturer, aging of the prescription, or other external factors. Therefore, we combine intact and degraded insulin and study its effect on solution viscosity. Therefore, by characterizing the viscosity of insulin mixtures we can determine a limit-of-detection in which PD can determine protein degradation in a mixed sample.

[0107] In particle diffusometry, we calculate the diffusion coefficient of particles in solution using correlation analysis (Clayton, et al., *Biomicrofluidics* 2016, 10, 1-15). More specifically, we record a series of images of a species of particles undergoing Brownian motion in a quiescent solution (FIG. 1). Following, these images are partitioned into smaller pixel² areas, known as interrogation areas. The size of the interrogation area is defined so that there are 8-10 particles are located in each partition. To perform cross-correlation on the interrogation areas, we correlate a first image, at time t, with a second image at time t+Δt. Cross-correlation is fundamental to determine ensemble particle displacement between two sequential images (FIG. 2). The further the particle displacement during Δt, the broader the cross-correlation peak is. In order to quantify the cross-correlation peak to calculate diffusion coefficient, we determine the width of the peak, s_a (pixels) at a height of 1/e. We additionally perform autocorrelation on the images. Autocorrelation instead correlates the interrogation window at time t with itself (FIG. 2). The autocorrelation peak width, s_a , is taller and narrower when compared to the cross-correlation peak. Using this information, we calculate the diffusion coefficient using the rearranged equation derived from Olsen and Adrian (Olsen, et al., *Exp. Fluids* 2000, 29, S166-S174):

$$D = \frac{s_e^2 - s_a^2}{16M^2\Delta t} \quad (1)$$

where M is the magnification of the microscope objective. Because the peak width has units of pixels, using Equation 1, we can see that the squared difference in the peak widths, $s_e^2 - s_a^2$, corresponds to the change in the cross-sectional area of the correlation peak at 1/e. By experimentally determining the diffusion coefficient from the particle images, we can algebraically rearrange the Stokes-Einstein relationship (Equation 2) in order to calculate the viscosity, η , of a solution (A. Einstein, *Ann. Phys.* 1905, 17, 549).

$$\eta = \frac{kT}{6\pi Da} \quad (2)$$

where, k is the Boltzmann constant, T is the absolute temperature, and a is the hydrodynamic radius of the spheres in the protein solution. We must assume in this instance that all particles in the solvent have the same hydrodynamic radius, a, and undergoing a constant temperature, T.

[0108] We are more specifically interested in how the presence of protein and how protein folding state alters solution viscosity. Therefore, we analyze the viscosity of the solutions in terms of relative viscosity rather than the magnitude. We can measure this by algebraic manipulation of Equation 2, where η_0 is the viscosity of the solution without protein (i.e. the solvent), but does include the 200 nm particles.

$$\frac{\eta}{\eta_0} = \frac{D_0}{D} \quad (3)$$

[0109] Particle Brownian motion was measured first in solvent to determine a baseline viscosity η_0 . These particles are added to the solvent in a concentration that is high enough to obtain statistically relevant results using particle diffusometry while limiting hydrodynamic particle interactions. To determine that we limit the effect of particle-particle interactions for our viscosity measurements, we use the relationship from Batchelor for a dilute monodisperse species of particles,

$$D_0 = D_{0*}(1+k\phi) \quad (4)$$

where D_0 is the effective diffusion coefficient from the addition of the polystyrene spheres, D_{0*} is the diffusion coefficient of the solvent, k is the type-specific constant where we use a value of 2, and ϕ is the volume fraction of the particles in solution (Batchelor, *J. Fluid Mech.* 1977, 83(01), 97; Elimelech, et al., in *Particle Deposition & Aggregation: Measurement, Modelling and Simulation*; 1998; pp 93-96). From Equation 4, the percent change in the diffusion coefficient due to the introduction of particles at a concentration of 2.88×10^8 particles/mL is 0.0025%. The hydrodynamic interactions of the particles may be considered negligible when this value is less than 0.01% (Elimelech, et al., 1998).

[0110] Preparation of Proteins for Viscosity Measurements

[0111] Bovine serum albumin fraction V (Dot Scientific, Batavia, Ill.) was solubilized in 1xPBS, pH 7.4. All intact samples were maintained at 4° C. prior to imaging. To denature BSA, protein samples were heated to 95° C. for 2 hours. Additionally, three different insulin solutions were studied in this work. The first insulin solution, from bovine pancreas (Sigma Aldrich, St. Louis, Mo., USA), was solubilized in 1xPBS with 1% glacial acetic acid, pH 2.5, in accordance with manufacturer instructions. These insulin sample was used to study protein folding state in acidic conditions. The second insulin sample, also from bovine pancreas, was supplied in 25 mM HEPES, pH 8.2 (Sigma Aldrich, St. Louis, Mo., USA), and further diluted in the same buffer. This second insulin solution was used to study insulin state at slightly basic conditions. The third insulin sample was used to study the impact that PBS and HEPES would make on insulin folding state. Insulin in 25 mM HEPES was lyophilized overnight, and resuspended the solution in a 1% glacial acetic acid to lower the pH to 2.5. All intact insulin samples were stored at 4° C. prior to imaging. Denaturation of insulin occurred by heating samples at 95° C. for 2 hours. Further, to determine the sensitivity of insulin degradation in sample, mixtures of intact and denatured insulin at both pH 8.2 and 2.5 were combined volumetrically at 100:0, 90:10, 80:20, 70:30, 60:40, 50:50, 40:60, 30:70, 20:80, 10:90, and 100:0, v/v, denatured:native.

[0112] A280 spectral reading is used to determine all protein concentrations. Each protein sample was measured three times on a Nanodrop 2000 (Thermo Scientific, Erie, N.Y., USA) and measurements were averaged to determine final protein concentration.

[0113] Native polyacrylamide gel electrophoresis (PAGE) was performed as a gold-standard method to determine protein folding state. Protein samples mixed with 4x native loading buffer were introduced to precast polyacrylimide gels (Mini-PROTEAN TGX, Bio-rad, Hercules, Calif., USA). Gels was developed at 120V for 1 hour and 20

minutes in 4° C., followed by staining in GelCode™ blue (ThermoFisher Scientific, Erie, N.Y., USA) for thirty minutes, and de-stained in deionized water overnight. All protein gels were imaged on a LI-COR Odyssey (Lincoln, Nebr., USA).

[0114] Performing Experimental Particle Diffusometry Measurements

[0115] Particles of 200 nm (Fluoro-max red dyed aqueous spheres, Thermo Scientific, Erie, N.Y., USA) were washed in either HEPES pH 8.2 or 1×PBS prior to use by centrifugation at 13,000×g for 15 minutes. Washed particles were added to protein solutions immediately prior to imaging at a final particle concentration of 2.88×10^8 particles/mL. All protein solutions were stored at 4° C. prior to imaging.

[0116] A simple fluid well was made by punching a 6 mm diameter through hole (120 μm thickness) in double-sided tape (Therm-O-Web, Wheeling, Ill.) and adhering the tape to a cover glass slide (thickness no. 1, Thermo Scientific, Erie, N.Y., USA). 3 μL of sample (protein solution plus nanoparticles) was introduced to the fluid well and sealed off with a second piece of cover glass, limiting convective evaporation. The sample was imaged using an inverted fluorescence microscope (Nikon TE-2000 U, Nikon, Japan) equipped with an X-cite lamp with 40× magnification. Images were recorded using a PCO 1600 CCD camera (PCO, Kelheim, Germany) with an 800×800 pixel² imaging window with 2×2 binning at 12.5 fps at the vertical middle plane of the chip (to ensure that particle diffusion was unhindered by the glass slides). We experimentally determined that a frame rate of 12.5 fps was rapid enough to capture particle Brownian motion but slow enough to allow the particles to displace measurably between consecutive frames. We imaged particle motion in 3 separate spatial locations of the fluid well to account for any spatial inhomogeneity that may occur. In each of these locations we made measurements at 3 different time-points to account for any temporal inhomogeneity. This approach provides us with a global view of viscosity measurements and any potential variations in it.

[0117] As this method uses volumetric illumination, all particles in the field of view were imaged, including those in front of and behind the microscope focal plane. However, as particles get farther from focus, their contribution to the correlation function decreases in a known way according to an expression derived by Meinhart et al. (Meinhart, et al. *Meas. Sci. Technol.* 2000, 11, 809-814). The effective measurement depth here (depth of correlation in PIV literature) is calculated to be 4.2 μm. This depth of correlation is located at a distance where the peak intensity of the particle image is found to be less than 1% of the peak intensity when the particle is perfectly in focus. Particle images were processed and auto and cross-correlation was performed using an in-house MATLAB code in order to determine the diffusion coefficient. 64×64 pixel² interrogation windows containing, on average, 8-10 particles were used for 100 image frame stacks (~8 seconds of data) for a high signal-to-noise ratio while maintaining a statistically relevant number of data points. Nine repetitions, where 100 images constituted an individual measurement, were performed for every individual sample. A two-dimensional Gaussian curve fit was used to calculate the orthogonal profile of the auto- and cross-correlation peaks for both the XZ- and YZ-planes. The width of the correlation peak is defined by 1/e and the width of the XZ- and YZ-Gaussian curves are averaged as one peak width value. To compare all viscosity measure-

ments from the PD measurements, student t-tests were performed between each and every measurement. A 95% confidence interval ($\alpha=0.05$) was used with a Bonferroni adjustment of α/n

[0118] Lower Limit of Detection Measurement

[0119] The lower limit of detection (LLOD) was calculated according to the equations found in literature.^{39,40} First, the limit of blank (LOB) was calculated by:

$$\text{LOB} = \text{mcan}_{\text{blank}} + 1.645(\text{SD}_{\text{blank}}) \quad (5)$$

where the $\text{mean}_{\text{blank}}$ is the mean value of the viscosity of 200 nm particles in buffer (sans protein), and SD_{blank} is the standard deviation of that same sample. From calculating the LOB we calculate the LLOD as:

$$\text{LLOD} = \text{LOB} + 1.645(\text{SD}_{\text{low concentration sample}}) \quad (6)$$

where the $\text{SD}_{\text{low concentration sample}}$ is the standard deviation of a low concentration analyte, here being the viscosity measurement of the lowest concentration of the protein measured with PD for every data set. Therefore, our LLOD is expressed as a relative viscosity value.

[0120] Non-Specific Protein Adsorption on Particles

[0121] To determine the extent of BSA nonspecific adsorption onto the 200 nm particle surface, particles suspended in all concentrations of the BSA solutions studied (0.01-10 mg/mL) at a final volume of 100 μL were incubated together for 1 hour. The particle-protein solutions were centrifuged at 13000×g and resuspended in 100 μL three times, with a final resuspension in a final volume of 15 μL of 1×PBS. This procedure was performed in triplicate. Particles were then combined with 4×SDS-PAGE loading buffer and boiled at 95° C. for 5 minutes. Samples were run on an SDS-PAGE gel for 1 hour and 20 minutes at 120 V at room temperature. The SDS-PAGE gel was stained with coomassie (GelCode Blue, ThermoFisher Scientific, Erie, N.Y., USA) for thirty minutes with gentle rocking followed by destaining in deionized water overnight. Gels were imaged with a LI-COR Odyssey. To compare the levels of protein present in the SDS-PAGE samples, the integrated pixel intensity of each protein band was found using LI-COR Odyssey system software. The integrated pixel intensity was used to back calculate concentrations of protein present in the band by also running known BSA “standards” at concentrations of 0.005, 0.0075, 0.01, 0.05, 0.1, and 0.25 mg/mL. The values for different protein concentrations from the SDS-PAGE gels for denatured and native protein were compared with a Tukey multiple comparison two-way ANOVA with a confidence level of 95%. The two-way ANOVA investigated how either native versus denatured protein affected adsorption to the particles as well as how different concentrations affect protein adsorption.

[0122] FITC Staining of Protein on Particles

[0123] Protein-particle solutions were stained in fluorescein isothiocyanate (FITC) to visually confirm protein content in the particle solution under fluorescence microscopy. FITC was dissolved at 1 mg/mL in DMSO prior to staining. Particle-protein solutions were adjusted to 0.1 M sodium carbonate. The 1 mg/mL dissolved FITC was added to the protein-particle solution at a 1:20 v/v, respectively, and incubated in the dark by rotation for 8 hours at 4° C. Following, NH_4Cl was added to the aliquots to a final volume of 50 mM and incubated in the dark by rotation for 2 hours at 4° C. For washing off excess protein to analyze nonspecifically adsorbed protein on the particle surface, particles were washed three times by centrifugation at 13

000×g and suspended to their same initial volume in 1×PBS. The fluorescent stained samples were imaged using the inverted fluorescence microscope (Nikon TE-2000U, Nikon, Japan) equipped with an X-cite lamp with 40× magnification on an Alexa 488 filter cube. Images were recorded with a DS2 camera (Nikon, Japan) and NIS Elements software (Nikon, Japan).

Results and Discussion

[0124] Investigating the Viscosity of BSA Solutions

[0125] BSA is used as a model protein to perform protein viscosity characterization studies in the PD system. The two initial parameters of interest are the effect of (1) concentration and (2) folding state of BSA on solution viscosity. To investigate the differences between native and denatured BSA, we perform a native PAGE on solutions of BSA at 0.25 mg/mL with and without heat treatment (FIG. 3A). As a consequence of aggregation that occurs among semiflexible polypeptide chains during heat denaturation, the denatured BSA is not electrophoretically mobile as it is too large to penetrate through the polyacrylamide gel. In contrast, native BSA displays several distinct bands at molecular weights that likely correspond to the presence of monomers, dimers, and oligomers in the BSA solution (Sayedmohammad, et al., *Biosci. Rep.* 2016, 32(2), 1-13). A solution of denatured and native BSA solution at a 1:1 v/v ratio shows features of both electrophoretically immobile denatured BSA and the presence of BSA monomers, dimers, and oligomers (FIG. 3A).

[0126] Measurements of the relative viscosity of solutions of BSA with and without heat treatment were performed using PD (FIG. 3B). Measurements of heat denatured BSA solutions could only be performed up to a concentration of 5 mg/mL as gelling occurred in samples above this concentration, causing significant errors in pipetting. We observe that the viscosity of denatured BSA solutions dramatically increases as a function of concentration (FIG. 3B). PD can be used to determine differences in viscosity between solutions of native and denatured BSA at concentrations of approximately 0.3 mg/mL and greater ($p < 0.001$ for 0.3 and 0.6 mg/mL and $p < 0.0001$ for 1 mg/mL and greater), raw PD data in Tables 1 and 2).

TABLE 1

Relative BSA Viscosity Measurements (Low Concentrations). Raw data values for the relative viscosity of low concentrations of native and denatured BSA using PD (inset on FIG. 3B).						
Concentration (mg/ml)	0.003 ± 0.000	0.036 ± 0.004	0.068 ± 0.007	0.127 ± 0.003	0.324 ± 0.003	0.613 ± 0.016
Native	1.00 ± 0.04	1.16 ± 0.05	1.11 ± 0.02	1.09 ± 0.02	1.10 ± 0.02	1.14 ± 0.02
Denatured	1.00 ± 0.04	1.09 ± 0.05	1.17 ± 0.09	1.07 ± 0.06	1.17 ± 0.05	1.18 ± 0.02

TABLE 2

Relative BSA Viscosity Measurements (High Concentrations). Raw data values for the relative viscosity of high concentrations of native and denatured BSA using PD (FIG. 3B).					
Concentration (mg/ml)	1.184 ± 0.011	2.914 ± 0.035	5.622 ± 0.007	8.170 ± 0.019	10.451 ± 0.079
Native	1.09 ± 0.02	1.09 ± 0.02	1.14 ± 0.04	1.10 ± 0.02	1.16 ± 0.03
Denatured	1.23 ± 0.05	1.59 ± 0.08	3.48 ± 0.42	N/A	N/A

TABLE 3

Integrated Intensity Measurements.*						
Concentration (mg/ml)	0.003 ± 0.000	0.036 ± 0.004	0.068 ± 0.007	0.127 ± 0.003	0.324 ± 0.003	0.613 ± 0.016
Native post- wash (mg/ml)	0.003 ± 0.001	0.012 ± 0.004	0.011 ± 0.010	0.010 ± 0.003	0.020 ± 0.016	0.014 ± 0.013
Denatured post wash (mg/ml)	0.003 ± 0.001	0.006 ± 0.001	0.008 ± 0.004	0.014 ± 0.008	0.024 ± 0.029	0.005 ± 0.004
Concentration (mg/ml)	1.184 ± 0.011	2.914 ± 0.035	5.622 ± 0.007	8.170 ± 0.019	10.451 ± 0.079	
Native post- wash (mg/ml)	0.012 ± 0.009	0.018 ± 0.014	0.024 ± 0.008	0.015 ± 0.008	0.011 ± 0.012	
Denatured post wash (mg/ml)	0.050 ± 0.083	0.142 ± 0.236	0.054 ± 0.070	N/A	N/A	

*LI-COR Odyssey software is used to determine the integrated intensity and back calculate the amount of nonspecifically adsorbed BSA onto polystyrene surfaces post-washing. All calculations were based on a standard curve of integrated intensity bands on an SDS-PAGE of known BSA concentrations of 0.005, 0.0075, 0.01, 0.05, 0.1, and 0.25 mg/ml ($R^2 = 0.99$). All values are normalized by the integrated intensity signal measured from the background signal of the SDS-PAGE gel.

[0127] For native BSA, we observe no increase in the solution viscosity at increasing BSA concentrations (p -value > 0.05). We experimentally measure the lower limit of detection (LLOD) needed to differentiate between native and denatured BSA. The LLOD, measured as the relative viscosity, is a value of 1.12; in this case meaning that PD can measure the viscosity of denatured BSA at concentrations of 0.3 mg/mL and greater. However, this LLOD will change depending on the pH and buffer conditions which BSA is subjected to. Further, individual native BSA proteins, like other globular proteins, can be modeled as hard rigid spheres moving in space. On the other hand, denatured BSA, similarly to other denatured proteins, is likely better-described as a discrete semiflexible polymer (Livadaru, et al., *Macromolecules*, 2003, 36, 3732-3744; Choi, et al., *Structure*, 2011, 19, 566-576). Thus we speculate that the non-linear trend of increasing viscosity with increasing concentration of denatured protein in FIG. 3B is likely due to increases in unfolded protein aggregation at increasing concentrations.

[0128] To validate the PD measurements, we use microrheology to measure BSA solution viscosity and correlate the results with the PD outputs. Microrheology is an established method for passive viscosity measurements applying the fundamentals of particle tracking (Josephson, et al. *J. Rheol.* 2016, 60, 531-540; Squires, et al, *Annu. Rev. Fluid Mech.* 2010, 42, 413-438). The PD and microrheology BSA solution viscosity measurements are positively correlated (Clayton, et al., *Lab Chip*, 2017, 17, 4148-4159). For denatured solutions, the Pearson's correlation coefficient between microrheology and PD are 0.96. The correlation of the native solution viscosity measurements has a Pearson's correlation coefficient of 0.78. The lower correlation coefficient in native BSA solutions is to be expected based on the assumptions used in colloidal-based microrheology mea-

surements. Microrheology assumes a uniform charge distribution for globular proteins; however, this assumption fails for proteins like BSA (Amin, et al., *Curr. Opin. Colloid Interface Sci.* 2014, 19, 438-449). This would lead to a larger discrepancy between measurements (lower Pearson's correlation coefficient). The implications of the differing correlations for native versus denatured solution viscosity potentially indicates higher variability in measurements for microrheology and possibly for PD.

[0129] Non-Specific Protein Adsorption on Viscosity Measurements

[0130] The relative change in solution viscosity that we calculate in FIG. 3B may not be a function of protein denaturation alone. Particles without chemical surface modifications are likely to have non-specific adsorption of proteins to their surfaces, thus increasing the particles' hydrodynamic radii (Clayton, et al., *Biomicrofluidics* 2016, 10, 1-15). As a particle's radius increases, its diffusion coefficient decreases according to the Stokes-Einstein equation. We see the particle size may be increasing in the presence of BSA. The LLOD is found to be at a relative viscosity of 1.12, indicating that the solution viscosity of denatured BSA would have to be 1.12 times greater than the bare 200 nm particle size to see a statistically significant signal difference. Therefore, the effect of low levels of protein adsorption onto particle surfaces, even at low protein concentrations and regardless of protein folding state, may contribute to lower sensitivity of the PD measurement. To study the effect that non-specific adsorption of proteins onto our particles has on PD measurements, we first investigate whether or not native BSA non-specifically adsorbs onto unmodified particle surfaces. Polystyrene particles were incubated with fluorescently labeled FITC-BSA, imaged, washed to remove the excess BSA, and imaged again to visualize any remaining fluorescent protein that is attached to the particle surface (FIG. 4A). In FIG. 4A it is evident that in the unwashed sample FITC-BSA is dispersed throughout, as indicated by green fluorescence (FITC). After removing the free BSA, the FITC signal is localized to the particle surfaces. This confirms that non-specific adsorption of BSA is, in fact, occurring on these unmodified red fluorescent polystyrene spheres.

[0131] We perform a semi-quantitative SDS-PAGE analysis to determine the degree of which BSA non-specifically adsorbed to the particle surface between different sample groups. Particles are incubated with either native or denatured BSA solutions at varying protein concentrations (0.01-10 mg/mL), washed, boiled in the presence of SDS, and analyzed. SDS-PAGE analysis of the boiled protein-particle samples shows that the protein can be stripped from the particles and visualized with coomassie (FIG. 4B). From the SDS-PAGE, the integrated pixel intensities of all the protein bands are measured with image processing (values in Table 3) and are compared using a two-way ANOVA with a post-hoc Tukey test to determine if protein folding state or protein concentration have an effect on non-specific adsorption onto the particle surface. We find no statistically significant difference (p -value >0.05) among the integrated pixel intensity values of the protein bands for native BSA and denatured BSA, respectively at all concentrations. This indicates that protein folding state does not change the amount of protein non-specifically adsorbed to the particle. Furthermore, the integrated intensity values of the SDS-PAGE bands at all concentrations (0.01-10 mg/mL) relative

to one another are also not statistically significantly different (p -value >0.05), indicating that concentration does not play a role of the quantity of non-specific protein adsorption onto the particles. Together we take these results to mean that similar amounts of protein non-specifically adsorb onto particle surfaces regardless of folding state (denatured vs. native protein) or concentration of protein in solution. Thus, we assume that all particles, regardless of protein treatment, undergo the same surface adsorption, and the differences in diffusion coefficient that we measure with PD indicates changes in the viscosity of the protein-particle solutions, rather than differences in particle size due to non-specific adsorption. This also indicates that differences in solution viscosity at lower protein concentrations maybe obtainable with particle surface modifications that are meant to block non-specific adsorption.

[0132] Viscosity Measurements of Insulin Solutions

[0133] Having determined that PD can readily determine differences of viscosity between native and denatured BSA solutions, we sought to characterize the change in solution viscosity of native and denatured state of a more pharmacologically relevant protein, insulin. Insulin has vastly different physiochemical properties than BSA. The molecular weight of insulin is 5.8 kDa (BSA is 66.5 kDa) and is a heterodimer comprised of separate α and β subunits. When insulin is denatured, the protein separates into its two respective subunits due to the breakage of disulfide bonding separating into two 21 and 30 amino acid polypeptide chains, respectively. In contrast, BSA when unfolded is a single 607 amino acid polypeptide chain.

[0134] There are currently multiple formulations of insulin produced by biopharmaceutical companies. As many of these formulations are proprietary and the exact formulation is not public information, we measured the viscosity of insulin solutions comprised of different buffers (HEPES and PBS) at two different pH values (2.5 and 8.2). Therapeutic insulin is often found at different pH depending on the application. In our work, we use a pH of 2.5 and 8.2 first to follow manufacturer's instructions for protein dilution and resuspension. These pHs are also relevant in a clinical setting. A pH of 8.2 is often used for therapeutic insulin crystals. Further, a pH of 2.5 is used, by USP guidelines, for acidified insulin.

[0135] Proper folding of insulin in PBS pH 2.5 was verified by native PAGE. The relative viscosities of native and degraded insulin at varying concentrations are measured using PD (FIG. 5A-5C). We observe that, similar to BSA, the viscosity of denatured insulin solutions dramatically increases as the concentration of the protein increases (raw data in Table 4). From this the experimentally measured LLOD of insulin in PBS is at a relative viscosity of 1.09, which is similar to our measurement for BSA LLOD (1.12). This relative viscosity measurement occurs at a concentration of denatured insulin in PBS pH 2.5 somewhere below 2 mg/mL, indicating that we can detect significant differences in the viscosity of denatured compared to native insulin at concentrations of 2 mg/mL and greater ($p < 0.0001$, FIG. 5A), but not below.

[0136] Interestingly, changes in the relative viscosity of denatured insulin as a function of concentration varies with buffer and pH. After performing the insulin viscosity study in PBS, PD is used to assess the viscosity of insulin in HEPES pH 2.5. Significant differences in the viscosity of denatured and native insulin are detectable at concentrations

of 4 mg/mL and greater when solubilized in HEPES at pH 2.5 (FIG. 5B). The LLOD of PD measurements of the relative insulin viscosity of HEPES pH 2.5 is 1.07, which occurs at the 4 mg/mL denatured protein concentration. PD measurements of relative viscosity of native insulin in HEPES pH 2.5 do not significantly vary as a function of concentrations (PD data in Table 5). The measurements of BSA and insulin in 1xPBS at pH 2.5 and insulin in HEPES at pH 2.5 suggest that PD can be used to measure changes in relative viscosity with a LLOD of 1.12.

TABLE 4

Relative Viscosity of Insulin in PBS. Raw data values for the relative viscosity of native and denatured insulin suspended in 1X PBS pH 2.5 using PD (FIG. 5A).						
Concentration (mg/ml)	0.00 ± 0.00	0.61 ± 0.04	2.06 ± 0.07	3.1 ± 0.02	6.12 ± 0.08	
Native	1.00 ± 0.03	1.01 ± 0.04	0.96 ± 0.03	1.01 ± 0.04	0.97 ± 0.02	
Denatured	1.00 ± 0.01	1.03 ± 0.01	1.33 ± 0.06	1.48 ± 0.07	2.72 ± 0.06	

TABLE 5

Relative Viscosity of Insulin in HEPES pH 2.5. Raw data values for the relative viscosity of native and denatured insulin suspended in 2.5 mM HEPES pH 2.5 using PD (FIG. 5B).						
Concentration (mg/ml)	0.00 ± 0.00	0.88 ± 0.06	2.08 ± 0.01	4.08 ± 0.11	5.80 ± 0.05	7.96 ± 0.03
Native	1.00 ± 0.03	0.99 ± 0.03	1.05 ± 0.04	0.97 ± 0.03	0.97 ± 0.02	1.09 ± 0.03
Denatured	1.00 ± 0.03	1.07 ± 0.05	1.00 ± 0.04	1.26 ± 0.08	1.95 ± 0.14	3.27 ± 0.26

TABLE 6

Relative Viscosity of Insulin in HEPES pH 8.2. Raw data values for the relative viscosity of native and denatured insulin suspended in 2.5 mM HEPES pH 8.2 using PD (FIG. 5C).						
Concentration (mg/ml)	0.02 ± 0.01	1.17 ± 0.04	2.74 ± 0.08	5.07 ± 0.01	7.48 ± 0.05	9.73 ± 0.04
Native	1.00 ± 0.02	1.02 ± 0.01	1.03 ± 0.02	1.01 ± 0.01	1.03 ± 0.02	1.05 ± 0.02
Denatured	1.00 ± 0.02	1.02 ± 0.02	1.01 ± 0.00	1.12 ± 0.01	1.21 ± 0.06	1.45 ± 0.03

[0137] We also measured the relative viscosity of insulin solutions in HEPES pH 8.2. Measured changes in relative viscosity of denatured insulin show a much less drastic nonlinear increase in viscosity at increasing concentrations as compared to the PBS and HEPES pH 2.5 cases. In the HEPES pH 8.2 buffer condition, PD measures the difference in viscosity between native and degraded insulin at a concentration of 5 mg/mL and greater ($p < 0.0001$, FIG. 5C) which is where PD reaches its LLOD. Additionally, following the same trend as the PBS and HEPES pH 2.5 cases, there is no discernible change in relative viscosity between all concentrations of native insulin in HEPES pH 8.2 over the range of concentrations measured (PD data in Table 6). Taking these results together, we see that that denatured insulin solubilized in buffers which are closer to physiological pH have less dramatic measurable changes in viscosity. Likewise, the buffer/salt content, such as PBS versus

HEPES, has an effect on the viscosity of denatured insulin solutions as well, suggesting that PD can detect how the solubility of denatured protein changes as a function of changes in buffer conditions.

[0138] We attribute these differences in changes in relative viscosity to the interaction of the denatured protein with the various ions and salts in the different buffer and pH solutions. Ion and salt content of solutions are known to affect protein morphology, interacting with the exposed amino acid side chains of the proteins to either shield or change individual amino acid charge. The isoelectric point of insulin is pH 5.4; thus the overall charge of insulin is positive in the acidic pH and negative in the basic buffer. These molecular interactions are likely having a direct effect on how the denatured polypeptide chains of insulin are interacting with each other in solution, and in turn, affecting measurements of solution viscosity obtained with PD. Additionally, at the pH of 2.5 the insulin has a net positive charge. At this pH the insulin could interact electrostatically with the negatively charged 200 nm particles (zeta potential of -40 mV). On the other hand, insulin at pH 8.2 has a net negative charge and could exhibit repulsive interactions with the particles. This effect could also be attributing to differences in the viscosity measurements, where the insulin suspended in solutions with pH values below the isoelectric point can be expected to exhibit greater viscosity changes than those suspended in solutions with a pH above the isoelectric point. We conclude that buffer conditions play a major role in the viscosity of denatured protein solutions, and speculate that different biopharmaceutical formulations of insulin would have different absolute viscosity measurements. Regardless, as the concentration of degraded insulin in a sample increases, the relative viscosity of the solution is expected to markedly increase to detectable levels.

[0139] Studies of Mixtures of Insulin

[0140] Prescription insulin is stored at concentrations between 100 units per mL to 200 units per mL, which is equivalent to 3.5-7 mg/mL, assuming all insulin is native at the time of manufacturing and packaging. However, it is unlikely in practice that prescription insulin will be either 100% degraded or 100% native. In fact, many studies indicate that a potency of $>95\%$ is found to be acceptable for biotherapeutic insulin (Kerr, et al., *J. Diabetes Sci. Technol.* 2013, 7, 1595-1606). We therefore sought to measure the changes in relative viscosity of mixtures of varying ratios (v/v) of native and denatured insulin at a consistent concentration of 6 mg/mL (to remain within the range of prescription insulin). Like BSA (FIG. 3A) most denatured insulin does not enter the PAGE gel, and remains at the entrance to the gel channel (FIG. 6A, red box), indicating aggregation of denatured protein. In contrast, the native protein is electrophoretically mobile and moves into the PAGE gel (FIG. 6A, blue box). Consistent with the varying ratio of native to denatured insulin, higher intensity bands within the gel channel are present in insulin mixtures containing larger ratios of native insulin, whereas higher intensity bands at the channel entrance correlate with larger volumes of denatured insulin.

[0141] To determine the relative viscosity of the varying insulin mixtures PD measurements are performed in both PBS pH 2.5 and HEPES pH 8.2. As expected, the relative viscosity of insulin solutions increases as the percentage of denatured insulin increases (FIGS. 6B and 6C). Insulin solutions in PBS pH 2.5 (FIG. 6B) show a more dramatic change in protein viscosity between each v/v ratio when

compared to insulin in HEPES pH 8.2 (FIG. 6C). This behavior is expected given our findings comparing exclusively denatured to exclusively native insulin solutions (FIGS. 5B and 5C). There is a significant difference in the relative viscosity of PBS insulin solutions starting at as little as 10% denatured insulin ($p\text{-value}=1\times 10^{-19}$). From this, we calculated our lower limit of detection of insulin in PBS to be below the 90:10 native to denatured insulin mixture. The relative viscosity change is 0.21, compared to the 100:0 native to denatured insulin mixture (PD data found in Table 7). Therefore, in PBS the viscosity measurements reach the 95% threshold needed for biotherapeutic insulin. In solutions of insulin in HEPES at pH 8.2 we detect a difference in relative viscosity of solutions with 50:50 native to denatured insulin mixture when compared to 100:0 (relative viscosity change of 0.1, PD data found in Table 8). This relative viscosity produces a less statistically significant measurement between native: denatured measurements. Therefore, future optimization can be performed to increase sensitivity in the measurement signal, such as using smaller diameter particles (i.e. 100 nm) or increasing measurement times (i.e. more images to perform correlation) (Clayton, et al., *Biomicrofluidics* 2016, 10, 1-15).

for formulation development and upscale manufacturing. Antibodies have molecular weights typically around 150 kDa (with 2 light chains and 2 heavy chains), which is much larger than BSA and insulin. Because of this, native antibodies are more likely to cause changes in concentration than smaller biotherapeutic proteins. Therefore, we use PD to study the effect of increasing concentration of native IgG antibodies on solution viscosity (raw data presented in Table 9). As expected, there is a gradual increase in solution viscosity as the concentration of antibodies is increased (FIG. 7). Performing a t-test between each concentration (with a Bonferroni adjustment of α/n), there is statistically significant differences in the relative viscosity of each concentration measured ($p<0.0001$ and $p<0.001$). A change in concentration of around 10 mg/mL produces changes in solution viscosity of around 0.14 ± 0.02 , which is above our LLOD. This is promising because mAb therapeutics remain far above this concentration. Therefore, PD can be used to measure high concentrations of antibody solutions for downstream applications in mAb formulation characterization.

[0144] Plasmid DNA Viscosity

[0145] FIG. 8A shows relative solution viscosity was measured with PD and DLS as a function of increasing 3618

TABLE 7

Relative Viscosity of Insulin Mixtures in PBS. Raw data values for the relative viscosity of native and denatured insulin combinations (denatured:native) suspended in 1X PBS pH 2.5 using PD (FIG. 6B).										
100:0	90:10	80:20	70:30	60:40	50:50	40:60	30:70	20:80	10:90	0:100
2.87 ± 0.10	2.01 ± 0.20	1.88 ± 0.08	1.91 ± 0.11	1.73 ± 0.18	1.64 ± 0.28	1.61 ± 0.19	1.45 ± 0.11	1.35 ± 0.07	1.25 ± 0.02	1.01 ± 0.04

TABLE 8

Relative Viscosity of Insulin Mixtures in HEPES. Raw data values for the relative viscosity of native and denatured (denatured:native) insulin combinations suspended in 2.5 mM HEPES pH 8.2 using PD (FIG. 6C).										
100:0	90:10	80:20	70:30	60:40	50:50	40:60	30:70	20:80	10:90	0:100
1.18 ± 0.05	1.15 ± 0.02	1.14 ± 0.04	1.14 ± 0.04	1.14 ± 0.03	1.13 ± 0.02	1.12 ± 0.04	1.12 ± 0.04	1.10 ± 0.03	1.08 ± 0.02	1.07 ± 0.01

TABLE 9

Relative Viscosity of IgG. Raw PD data for the relative viscosity of IgG (FIG. 7).						
Concentration (mg/ml)	0	10	20	30	40	50
Native	1.00 ± 0.03	1.14 ± 0.02	1.20 ± 0.03	1.35 ± 0.02	1.52 ± 0.04	1.61 ± 0.02

[0142] Monoclonal Antibody Viscosity

[0143] Monoclonal antibodies are stored at high concentrations for patient injection. These high concentrations lead to quite viscous solutions, which in turn cause issues with injecting the drug, requiring larger gauge needles and negatively affecting patient comfort. Viscous antibodies also cause difficulty in manufacturing handling, which is detrimental for efficient product output. With 70 mAb drugs expected to be on the market by 2020, there is an opportunity to design high throughput viscosity measurement systems

bp pRSET emGFP plasmid concentration. FIG. 8B shows Changes in solution viscosity as a function of circular plasmid DNA concentration by increasing 6162 bp pD444-SR plasmid concentration. Measurements were relative to QIAGEN elution buffer. $n=3$ independent experiments. FIG. 8C demonstrates that DLS and PD measurements were highly positively correlated. Pearson Correlation Coefficient=0.98.

[0146] FIG. 9A shows relative solution viscosity as measured with PD and DLS as a function of increasing 3618 bp pRSET emGFP linear plasmid concentration. FIG. 9B describes Changes in solution viscosity as a function of linear plasmid DNA concentration by increasing 6162 bp pD444-SR linear plasmid concentration. DNA concentrations below the critical concentration are marked by a dotted line. Measurements are relative to QIAGEN elution buffer. $n=3$ independent experiments. FIG. 9C demonstrates that DLS and PD measurements were highly positively correlated. Pearson Correlation Coefficient=0.85. The dashed lines indicate a 95% confidence interval.

[0147] To summarize, using particle diffusometry (PD), we have developed a method with which we can determine the degree of protein degradation. With PD we observe that native proteins show little-to-no change in viscosity up to concentration changes of approximately 10 mg/mL (FIGS. 3A-3B, 5A-5C and 7). This limit is likely to vary most with the size of the protein. However, heat denaturation of protein solutions produces measurable changes in sample viscosity as a function of increasing concentration (FIGS. 3A-3B and 5A-5C). This change in the viscosity occurs due to unfolding, aggregation of proteins during the denaturation process. As such, we observe that the concentration at which denatured insulin solutions exhibit viscosities significantly different from solutions with native protein is a function of solution buffer and pH (FIGS. 5A-5C). One important implication of these results is that quantitative measurements of protein degradation would require standards and controls with similar buffer formulations to be accurate. Regardless, these measurements are robust and allow for detection of as little as 10% denatured insulin in some formulations (FIGS. 6A-6C). These results are readily translated to other important biotherapeutic products, such as monoclonal antibodies, a significantly larger protein than insulin (FIG. 7) that are regularly administered to patients at high concentrations. As such, the viscosity of mAb solutions is a critically important parameter that affects the dosing strategy. Our measurements use sample volumes of 3 μ L and imaging times of 8 seconds. Our current algorithms implemented on an Intel® Core™ i5-3230M CPU at 2.60 GHz computer processor require approximately 18 seconds per sample. Thus time-to-result per sample is as low as 30 seconds and could be optimized to run even faster. A tool like PD would enable rapid, high throughput, and low volume measurements of biotherapeutic formulations, and may be implemented for formulations research and development, or in manufacturing and distribution settings. We also envision PD-enabled point of care diagnostics for clinics and patients. Integration of PD with small handheld devices would enable pharmacists and patients to track the viability of their protein-based prescriptions. Implementation of particle diffusometry for measuring the viscosity of biotherapeutic solutions could be used to optimize pharmaceutical formulations, track biotherapeutic stability throughout the manufacturing and distribution chain, and be used in clinical settings as measure of the efficacy of a biotherapeutic. Implementing these methods could potentially decrease prescription waste, decrease incorrect drug use, mitigate adverse reactions in patients, and provide new means for patients to control their own health and prescription monitoring.

[0148] Those skilled in the art will recognize that numerous modifications can be made to the specific implementations described above. The implementations should not be limited to the particular limitations described. Other implementations may be possible.

[0149] While the inventions have been illustrated and described in detail in the drawings and foregoing description, the same is to be considered as illustrative and not restrictive in character, it being understood that only certain embodiments have been shown and described and that all changes and modifications that come within the spirit of the invention are desired to be protected.

What is claimed is:

1. A method for measuring viscosity of a liquid comprising the steps of:
 - a. preparing a testing solution using said liquid with added uniformly sized particles of about 50 ~1,000 nm.
 - b. capturing a plurality of microscopic images of said particles in said testing solution over a period of time;
 - c. partitioning each of the plurality of images into interrogation regions and determining the average displacement of the particles in each of the interrogation regions of the plurality of images over said time period;
 - d. determining diffusion coefficient of the particles based on the average displacement of the particles; and
 - e. calculating viscosity of said liquid using determined diffusion coefficient with Einstein's diffusion equation.
2. The method of claim 1, wherein the uniformly sized particles are made of gold, silver, polystyrene, or similar structurally stable materials, wherein the particles are optionally labeled or magnetic.
3. The method of claim 1, wherein the liquid is a biomolecular composition selected from the group consisting of nucleic acid, amino acid, lipid, peptide, protein, antibody, enzyme, carbohydrate, DNA, RNA, polysaccharide, oligonucleotide, oligosaccharide, proteoglycans, and glycoprotein.
4. The method of claim 3, wherein said biomolecular composition is a biological therapeutics.
5. The method of claim 1, wherein the method is used for measuring structural and functional changes of a biomolecular composition of testing subject from a standard thereof, comprising the steps of:
 - a. measuring viscosity of the biomolecular composition of testing subject;
 - b. measuring viscosity of the standard biomolecular composition of testing subject; and
 - c. comparing viscosity of said biomolecular composition of testing subject with that of said standard, wherein finding of a substantial difference suggests structural and functional changes of said biomolecular composition of testing subject.
6. A method for measuring structural and functional changes of a biomolecular composition of testing subject from a standard thereof, comprising the steps of:
 - a. preparing a testing solution using said biomolecular composition with added uniformly sized particles of about 50~1,000 nm.
 - b. capturing a plurality of microscopic images of said particles of said testing solution over a period of time;
 - c. partitioning each of the plurality of images into interrogation regions and determining the average displacement of the particles in each of the interrogation regions of the plurality of images over said time period;
 - d. determining a diffusion coefficient based on the average displacement of the particles;
 - e. calculating viscosity of said biomolecular composition of testing subject using the determined diffusion coefficient with Einstein's diffusion equation;
 - f. obtaining viscosity of a standard biomolecular composition of testing subject by repeating steps a.-e.; and
 - g. comparing viscosity of said biomolecular composition of testing subject and that of said standard thereof, wherein finding of a substantial difference suggests structural and functional changes of said biomolecular composition of testing subject.

7. The method of claim 6, wherein said biomolecular composition comprises a biomolecule selected from the group consisting of nucleic acid, amino acid, lipid, peptide, protein, antibody, enzyme, carbohydrate, DNA, RNA, polysaccharide, oligonucleotide, oligosaccharide, proteoglycans, and glycoprotein.

8. The method of claim 6, wherein said biomolecular composition comprises a combination of two or more of biomolecules selected from the group consisting of nucleic acid, amino acid, lipid, peptide, protein, antibody, enzyme, carbohydrate, DNA, RNA, polysaccharide, oligonucleotide, oligosaccharide, proteoglycans, and glycoprotein.

9. The method of claim 8, wherein said biomolecular composition is prepared by combining individual components.

10. The method of claim 6, wherein said biomolecular composition is derived from bodily fluids, cell cultures, environmental samples, air samples, water samples, soil samples, or other matrices that contain biomolecules.

11. The method of claim 6, wherein said biomolecular composition is derived from a living organism including prokaryotic cells, eukaryotic cells, viruses, or prions.

12. The method of claim 6, wherein the biomolecular composition is a therapeutic for treatment of a disease.

13. The method of claim 12, wherein said biomolecular composition is an insulin formulation.

14. The method of claim 12, wherein said biomolecular composition is an enzyme or an antibody formulation.

15. The method of claim 12, wherein said biomolecular composition is a peptide, protein or glycoprotein formulation.

16. A method for detecting presence of bacterial, viral, protozoa, fungal, or other parasitic contamination of a liquid, comprising the step of:

- a. preparing a testing solution using said liquid with added uniformly sized particles of about 50 ~1,000 nm.
- b. capturing a plurality of microscopic images of said micro particles of said testing solution over a period of time;
- c. partitioning each of the plurality of images into interrogation regions and determining the average displacement of the particles in each of the interrogation regions of the plurality of images over said time period;
- d. determining diffusion coefficient of the particles based on the average displacement of the particles;
- e. calculating viscosity of said liquid using the determined diffusion coefficient with Einstein's diffusion equation;
- f. obtaining viscosity of a non-contaminated standard of said liquid by repeating steps a.-e.; and
- g. comparing viscosity of said liquid and that of said non-contaminated standard thereof, wherein finding of a substantial difference suggests presence of bacterial, viral, protozoa, fungal, or other parasitic contamination of said liquid.

17. The method of claim 16, wherein said liquid is for human or animal consumption.

18. The method of claim 16, wherein said liquid is selected from the group consisting of biological medicine, water, waste water of any source, fruit juice, vegetable juice, liquid food, and a liquid waste from a food or feed processing.

19. The method of claim 16, wherein the method is used for quality control of biological medicines, food and feeds during the process of manufacturing, distribution and consumption.

20. The method of claim 19, wherein the biological medicine is a biotherapeutic formulation.

* * * * *